

Kinetic theory analysis of steady evaporating flows from a spherical condensed phase into a vacuum

Yoshio Sone and Hiroshi Sugimoto

京大・工 曾根 良夫 杉本 宏

Department of Aeronautical Engineering, Kyoto University, Kyoto 606-01 Japan

Abstract

Steady evaporating flows from a spherical condensed phase into a vacuum are considered. On the basis of the Boltzmann-Krook-Welander equation, the behavior of the gas (the velocity distribution function as well as the density, velocity, and temperature) from the sphere to downstream infinity is analyzed numerically in detail for the whole range of the Knudsen number. An analytic solution is also given for small Knudsen numbers. The discontinuity of the velocity distribution function in the gas, a typical behavior of the gas around a convex body, is analyzed accurately. It extends, with appreciable size, to downstream infinity not only for intermediate and large Knudsen numbers but also even for rather small Knudsen numbers. The flow is highly in nonequilibrium over the whole field except for very small Knudsen numbers. The velocity and temperature at downstream infinity take finite values, determined by the Knudsen number, except the temperature at zero Knudsen number.

I. INTRODUCTION

Considerable kinetic theory studies on gas flows around a condensed phase, where evaporation or condensation is taking place, have been carried out in the last twenty years (e.g., Refs. 1-34). Most of them are concerned with one-dimensional problems, but various important and interesting results are presented. The boundary conditions for hydrodynamic equation in the continuum limit on a interface between a gas and its condensed phase are derived from the analysis of a half-space problem of evaporation or condensation, where a semi-infinite expanse of a gas is considered.^{10,11,22,29,32} A steady evaporating flow of the half-space problem, determined by a parameter at downstream infinity in addition to the condition of the condensed phase, can neither be supersonic nor take a downstream pressure lower than some positive value p_{min} (Ref. 22). In the case where a plane condensed phase is adjacent to a vacuum, a time-dependent process occurs, and finally the whole field is filled with the gas and approaches a steady evaporating flow that is sonic and takes the pressure p_{min} at downstream infinity. The initial vacuum state disappears.

When a cylindrical or spherical condensed phase is set in an infinite expanse of a vacuum, its vapor gas expands into a wider region, and finally a steady evaporating flow into a vacuum will be established. The flow behavior depends on the Knudsen number of the condition on the condensed phase (the initial Knudsen number, for short). In the flow into a vacuum, as the gas going downstream, the mean free path increases indefinitely since the density decreases to zero, but the characteristic length becomes longer indefinitely corresponding to vanishing of the variation of the variables. According to the estimate by the spherically expanding isentropic flow in the continuum limit, the effective Knudsen number (the local mean free path divided by the local characteristic length), which characterizes the variation of the flow, increases indefinitely with the flow. Thus, various features are expected to be seen along the flow. Unfortunately

few are known about this interesting flow into a vacuum; some discussions were made about the deviation from local equilibrium well downstream of an isentropic expanding flow in the continuum limit.³⁵⁻³⁸ Recent engineering problems such as isotope separation by a laser beam³⁹ and vacuum vapor deposition require detailed information, at the level of the velocity distribution function, of the flow. In the present paper, therefore, we investigate a steady evaporating flow from a spherical condensed phase into a vacuum, mainly numerically, for the entire range of the initial Knudsen number to obtain the comprehensive information about the flow.

In the numerical analysis of the problem, there are two points to be treated carefully. First, as discussed in Refs. 34 and 40, the velocity distribution function has discontinuities in a gas around a convex body. Fortunately, a hybrid difference system (an ordinary difference system supplemented with a characteristic method) capable of describing the discontinuity accurately is devised in Ref. 34. This is applied to the present problem. Second, practical numerical computation has to be carried out over a finite domain. Unfortunately, in the present problem the flow field approaches a vacuum state at infinity fairly slowly. In order to obtain reliable results, therefore, we will analyze the problem for many cases of various domain sizes and examine the results carefully.

II. PROBLEM AND BASIC EQUATION

Consider a steady evaporating flow from a spherical condensed phase (radius: L , temperature: T_w , the saturation gas pressure at temperature T_w : p_w) into an infinite expanse of a vacuum. We investigate the behavior of the flow around the sphere for a wide range of the Knudsen number Kn_w (the mean free path at the equilibrium state at rest with temperature T_w and pressure p_w divided by the radius of the sphere) under the following assumptions: (i) the behavior of the gas is described by the Boltzmann-Krook-Welander (BKW or BGK) equation;⁴¹⁻⁴³ (ii) the gas molecules leaving the condensed phase constitute the corresponding part of the stationary Maxwellian distribution with pressure p_w and temperature T_w (the conventional boundary condition for evaporation and condensation). The extension of the result to a more general boundary condition will be given in Sec. VI.

The Boltzmann-Krook-Welander equation for a spherically symmetric steady flow is given as⁴⁴

$$\xi_r \frac{\partial f}{\partial r} + \frac{\xi_t^2}{r} \frac{\partial f}{\partial \xi_r} - \frac{\xi_r \xi_t}{r} \frac{\partial f}{\partial \xi_t} = A_{col} \rho (f_e - f), \quad (1)$$

$$f_e = \frac{\rho}{(2\pi RT)^{3/2}} \exp\left(-\frac{(\xi_r - u)^2 + \xi_t^2}{2RT}\right), \quad (2)$$

$$\rho = 2\pi \iint f \xi_t d\xi_r d\xi_t, \quad (3a)$$

$$\rho u = 2\pi \iint f \xi_r \xi_t d\xi_r d\xi_t, \quad (3b)$$

$$3\rho RT = 2\pi \iint f [(\xi_r - u)^2 + \xi_t^2] \xi_t d\xi_r d\xi_t, \quad (3c)$$

$$p = \rho RT, \quad (3d)$$

where r is the radial distance from the center of the sphere; ξ_r is the radial component of the molecular velocity; ξ_t is the magnitude of the molecular velocity normal to the radial direction,

that is, $(\xi_r^2 + \xi_t^2)^{1/2}$ is the molecular speed, which will be denoted by ξ for short; f is the velocity distribution function, which is a function of r, ξ_r , and ξ_t ; ρ is the density of the gas; u is the radial component of the flow velocity, which is the only nonvanishing component; T is the temperature of the gas; p is the pressure of the gas; A_{col} is a constant; R is the specific gas constant. The integration in Eqs. (3a)–(3c), and in what follows unless otherwise stated, is carried out over the range $(-\infty < \xi_r < \infty, 0 \leq \xi_t < \infty)$. The $A_{col}\rho$ is the collision frequency of a gas molecule, which is independent of molecular velocity for BKW equation. The parallel and normal temperatures T_{\parallel} and T_{\perp} , to the flow, are given by

$$\rho RT_{\parallel} = 2\pi \iint f(\xi_r - u)^2 \xi_t d\xi_r d\xi_t, \quad (4a)$$

$$\rho RT_{\perp} = \pi \iint f \xi_t^3 d\xi_r d\xi_t. \quad (4b)$$

Thus,

$$T = (T_{\parallel} + 2T_{\perp})/3. \quad (5)$$

The boundary condition on the condensed phase (at $r = L$) is

$$f = \frac{\rho_w}{(2\pi RT_w)^{3/2}} \exp\left(-\frac{\xi_r^2 + \xi_t^2}{2RT_w}\right), \quad (\xi_r > 0), \quad (6)$$

$$\rho_w = p_w/RT_w. \quad (7)$$

The condition at infinity ($r \rightarrow \infty$) is

$$f = 0, \quad (\xi_r < 0). \quad (8)$$

For the convenience of the following analysis, we introduce the following nondimensional variables:

$$r = L\hat{r}, \quad (9a)$$

$$\left. \begin{aligned} \xi_r &= (2RT_w)^{1/2} \zeta \cos \theta_{\zeta}, \\ \xi_t &= (2RT_w)^{1/2} \zeta \sin \theta_{\zeta}, \end{aligned} \right\} \quad (9b)$$

$$f = \frac{\rho_w}{2\pi(2RT_w)^{3/2}} \hat{f}, \quad (9c)$$

$$\left. \begin{aligned} \rho &= \rho_w \hat{\rho}, \quad u = (2RT_w)^{1/2} \hat{u}, \\ p &= p_w \hat{p}, \quad T = T_w \hat{T}. \end{aligned} \right\} \quad (9d)$$

With these new variables, the BKW equation (1) is reduced to

$$D\hat{f} = \frac{2}{\sqrt{\pi}Kn_w} \hat{\rho}(\hat{f}_e - \hat{f}), \quad (10)$$

where

$$D = \zeta \cos \theta_{\zeta} \frac{\partial}{\partial \hat{r}} - \frac{\zeta \sin \theta_{\zeta}}{\hat{r}} \frac{\partial}{\partial \theta_{\zeta}}, \quad (11a)$$

$$Kn_w = \frac{\ell_w}{L}, \quad \ell_w = \frac{(8RT_w/\pi)^{1/2}}{A_{col}\rho_w}, \quad (11b)$$

$$\hat{f}_e = \frac{2\hat{\rho}}{\pi^{1/2}\hat{T}^{3/2}} \exp\left(-\frac{\zeta^2 + \hat{u}^2 - 2\zeta\hat{u}\cos\theta_\zeta}{\hat{T}}\right). \quad (11c)$$

The ℓ_w is the mean free path at the equilibrium state at rest with pressure p_w and temperature T_w , and Kn_w is the Knudsen number at the state. In the new independent variables $(\hat{r}, \zeta, \theta_\zeta)$, the BKW equation contains only the derivatives with respect to \hat{r} and θ_ζ . The nondimensional macroscopic variables $\hat{\rho}, \hat{u}, \hat{T}$, and \hat{p} are related to \hat{f} as

$$\hat{\rho} = \iint \hat{f} \zeta^2 \sin\theta_\zeta d\zeta d\theta_\zeta, \quad (12a)$$

$$\hat{\rho}\hat{u} = \iint \hat{f} \zeta^3 \cos\theta_\zeta \sin\theta_\zeta d\zeta d\theta_\zeta, \quad (12b)$$

$$\frac{3}{2}\hat{\rho}\hat{T} = \iint \hat{f} \zeta^4 \sin\theta_\zeta d\zeta d\theta_\zeta - \hat{\rho}\hat{u}^2, \quad (12c)$$

$$\hat{p} = \hat{\rho}\hat{T}. \quad (12d)$$

The double integration with respect to ζ and θ_ζ in Eqs. (12a)–(12c), and in the following equations unless otherwise stated, is carried out over the domain ($0 \leq \zeta < \infty, 0 \leq \theta_\zeta \leq \pi$).

The nondimensional forms of the boundary conditions are, at $\hat{r} = 1$,

$$\hat{f} = \frac{2}{\sqrt{\pi}} \exp(-\zeta^2), \quad (0 \leq \theta_\zeta < \pi/2), \quad (13)$$

and, at infinity,

$$\hat{f} = 0, \quad (\pi/2 < \theta_\zeta \leq \pi). \quad (14)$$

The boundary-value problem [Eqs. (10), (13), and (14)] contains only a parameter, the Knudsen number Kn_w (Ref. 45). We will investigate the problem numerically for a wide range of the Knudsen number and clarify the comprehensive behavior of the evaporating flow from a spherical condensed phase into a vacuum.

Integrating Eq. (10) multiplied by $\zeta^2 \sin\theta_\zeta, \zeta^3 \cos\theta_\zeta \sin\theta_\zeta$, or $\zeta^4 \sin\theta_\zeta$ over the domain ($0 \leq \theta_\zeta \leq \pi, 0 \leq \zeta < \infty$), we obtain the following conservation equations:

$$\hat{\rho}\hat{u}\hat{r}^2 = Q/4\pi\rho_w(2RT_w)^{1/2}L^2, \quad (15)$$

$$\frac{d}{d\hat{r}}[(\hat{u}^2 + \hat{T}_\parallel/2)\hat{\rho}\hat{r}^2] = \hat{\rho}\hat{T}_\perp\hat{r}, \quad (16)$$

$$\hat{w}\hat{r}^2 = W/4\pi p_w(2RT_w)^{1/2}L^2, \quad (17)$$

$$\hat{w} = \iint \hat{f} \zeta^5 \cos\theta_\zeta \sin\theta_\zeta d\zeta d\theta_\zeta, \quad (18)$$

where Q and W are the mass flux and energy flux from the sphere respectively. Equations (15) and (17) will be used in an accuracy test of our computation.

The saturation gas pressure p_w is a function of T_w given by the Clausius-Clapeyron relation.⁴⁶ In the following analysis, however, the relation between p_w and T_w is never used, and thus p_w and T_w can be chosen freely in the results. Thus the result has wider application. Sec. VI is one of the examples.

III. METHOD OF NUMERICAL ANALYSIS

A. Preliminary remarks

In the numerical analysis of the boundary-value problem, Eqs. (10), (13), and (14), we have to limit the domain ($1 \leq \hat{r} < \infty$, $0 \leq \zeta < \infty$, $0 \leq \theta_\zeta \leq \pi$) of our interest to a finite domain ($1 \leq \hat{r} \leq \hat{r}_D$, $0 \leq \zeta \leq \zeta_D$, $0 \leq \theta_\zeta \leq \pi$). Since \hat{f} is seen to decay rapidly with ζ from our numerical tests, accurate computation of the problem can be carried out with a reasonable size of ζ_D . On the other hand, approach to the state at infinity as $\hat{r} \rightarrow \infty$ is rather slow, and therefore we will carry out detailed tests for various large \hat{r}_D and confirm the asymptotic behavior for large \hat{r} . This requires rather large computation.

Another difficulty in the numerical computation is the discontinuity of the velocity distribution function in the gas, which is pointed out and discussed in Refs. 34 and 40. The velocity distribution function on the condensed phase ($\hat{r} = 1$) is discontinuous at $\theta_\zeta = \pi/2$ (between the incoming and leaving molecules), and this discontinuity propagates into the gas along the characteristic of Eq. (10), i.e., $\hat{r} \sin \theta_\zeta = 1$. In the following numerical computation by a finite difference method, we have to take this discontinuity into account. Fortunately, a finite difference scheme capable of describing the discontinuity is developed in Ref. 34, which will be applied to the present computation.

B. Difference scheme and process of solution

The boundary-value problem, Eqs. (10), (13), and (14), is considered over a finite domain ($1 \leq \hat{r} \leq \hat{r}_D$, $0 \leq \zeta \leq \zeta_D$, $0 \leq \theta_\zeta \leq \pi$), where \hat{r}_D and ζ_D are chosen properly depending on situations. Let $(\hat{r}^{(i)}, \zeta^{(j)}, \theta_\zeta^{(k)})$ be the lattice points in the domain, where $i = 0, 1, \dots, I$ ($\hat{r}^{(0)} = 1$, $\hat{r}^{(I)} = \hat{r}_D$), $j = 0, 1, \dots, J$ ($\zeta^{(0)} = 0$, $\zeta^{(J)} = \zeta_D$), and $k = 0, 1, \dots, \widehat{K}, \dots, K$ ($\theta_\zeta^{(0)} = 0$, $\theta_\zeta^{(\widehat{K})} = \pi/2$, $\theta_\zeta^{(K)} = \pi$). For the convenience of analysis, the points $\hat{r}^{(i)}$, $\zeta^{(j)}$, and $\theta_\zeta^{(k)}$ are taken as the values of smooth functions $\hat{r}(s)$, $\zeta(s)$, and $\theta_\zeta(s)$ of a continuous variable s evaluated at integer points $s = i, j$, and k :

$$\hat{r}^{(i)} = \hat{r}(i), \quad \zeta^{(j)} = \zeta(j), \quad \theta_\zeta^{(k)} = \theta_\zeta(k). \quad (19)$$

The variables \hat{f} , $\hat{\rho}$, etc. at a lattice point are denoted by the superscripts corresponding to the lattice point:

$$\hat{f}^{(i,j,k)} = \hat{f}(\hat{r}^{(i)}, \zeta^{(j)}, \theta_\zeta^{(k)}), \quad \hat{\rho}^{(i)} = \hat{\rho}(\hat{r}^{(i)}). \quad (20)$$

Note that $\hat{f}_e^{(i,j,k)}$ depends on $\hat{r}^{(i)}$ only through $\hat{\rho}^{(i)}$, $\hat{u}^{(i)}$, and $\hat{T}^{(i)}$ [see Eq. (11c)].

We construct the discrete solution $\hat{f}^{(i,j,k)}$ of Eqs. (10), (13), and (14) as the limit of the sequence $\hat{f}_{(n)}^{(i,j,k)}$ ($n = 0, 1, 2, \dots$) obtained by the iteration process described below. Corresponding to Eq. (10), the following finite difference equation for $\hat{f}_{(n)}^{(i,j,k)}$ is adopted:

$$\begin{aligned} \zeta^{(j)} \cos \theta_\zeta^{(k)} \frac{\Delta_1^{(i,j,k)} \hat{f}_{(n)}^{(i,j,k)}}{(d\hat{r}/di)} - \frac{\zeta^{(j)} \sin \theta_\zeta^{(k)}}{\hat{r}^{(i)}} \frac{\Delta_2^{(i,j,k)} \hat{f}_{(n)}^{(i,j,k)}}{(d\theta_\zeta/dk)} \\ = \frac{2}{\sqrt{\pi} K n_w} \hat{\rho}_{(n-1)}^{(i)} (\hat{f}_{e(n-1)}^{(i,j,k)} - \hat{f}_{(n)}^{(i,j,k)}), \end{aligned} \quad (21)$$

where $\Delta_1^{(i,j,k)} \hat{f}_{(n)}^{(i,j,k)}/(d\hat{r}/di)$ and $\Delta_2^{(i,j,k)} \hat{f}_{(n)}^{(i,j,k)}/(d\theta_\zeta/dk)$, given explicitly below, correspond to $\partial \hat{f}_{(n)}/\partial \hat{r}$ and $\partial \hat{f}_{(n)}/\partial \theta_\zeta$, respectively.

We use the following formulae for the operators Δ_1 and Δ_2 :

$$\Delta_1^{(i,j,k)} \widehat{f}_{(n)} = \begin{cases} \frac{3}{2} \widehat{f}_{(n)}^{(i,j,k)} - 2 \widehat{f}_{(n)}^{(i-1,j,k)} + \frac{1}{2} \widehat{f}_{(n)}^{(i-2,j,k)}, & (2 \leq i \leq I, 0 \leq k \leq \widehat{K} - 1), & (22a) \\ \widehat{f}_{(n)}^{(1,j,k)} - \widehat{f}_{(n)}^{(0,j,k)}, & (i = 1, 0 \leq k \leq \widehat{K} - 1), & (22b) \\ -\frac{3}{2} \widehat{f}_{(n)}^{(i,j,k)} + 2 \widehat{f}_{(n)}^{(i+1,j,k)} - \frac{1}{2} \widehat{f}_{(n)}^{(i+2,j,k)}, & (0 \leq i \leq I - 1, \widehat{K} \leq k \leq K), & (22c) \end{cases}$$

$$\Delta_2^{(i,j,k)} \widehat{f}_{(n)} = -\frac{3}{2} \widehat{f}_{(n)}^{(i,j,k)} + 2 \widehat{f}_{(n)}^{(i,j,k+1)} - \frac{1}{2} \widehat{f}_{(n)}^{(i,j,k+2)}, \quad (22d)$$

$$(d\widehat{r}/di) = (d\widehat{r}/ds)_{s=i}, \quad (d\theta_\zeta/dk) = (d\theta_\zeta/ds)_{s=k}, \quad (22e)$$

$$\widehat{f}_{(n)}^{(i,j,K+1)} = \widehat{f}_{(n)}^{(i,j,K-1)}, \quad (22f)$$

and $\widehat{f}_{e(n-1)}^{(i,j,k)}$ is defined by Eq. (11c) where $\widehat{\rho}_{(n-1)}^{(i)}$, $\widehat{u}_{(n-1)}^{(i)}$, and $\widehat{T}_{(n-1)}^{(i)}$ are substituted for $\widehat{\rho}$, \widehat{u} , and \widehat{T} respectively. Equation (22f) corresponds to the symmetry relation with respect to θ_ζ around $\theta_\zeta = \pi$. The variable $\widehat{f}_{(n)}^{(I+1,j,k)}$ outside the domain is specified as a part of boundary conditions [Eq. (27b) below]. The $\widehat{f}_{(n)}^{(i,j,K+2)}$ does not appear since $\sin \theta_\zeta^{(K)} = 0$.

As explained in Sec. III A, \widehat{f} is discontinuous along $\widehat{r} \sin \theta_\zeta = 1$ ($0 < \theta_\zeta \leq \pi/2$). The difference formulae (22a)–(22d) should be modified when they consist of the data on both sides of the discontinuity. That is,

$$\Delta_1^{(i,j,k)} \widehat{f}_{(n)} = \begin{cases} A_1 \widehat{f}_{(n)}^{(i,j,k)} - A_2 \widehat{f}_{(n)}^{(i-1,j,k)} + A_3 \widehat{f}_{(n)}^{(i(k),j,k)+}, & (\widehat{r}^{(i-1)} > 1/\sin \theta_\zeta^{(k)} > \widehat{r}^{(i-2)}), & (23a) \\ A_4 (\widehat{f}_{(n)}^{(i,j,k)} - \widehat{f}_{(n)}^{(i(k),j,k)+}), & (\widehat{r}^{(i)} > 1/\sin \theta_\zeta^{(k)} > \widehat{r}^{(i-1)}), & (23b) \end{cases}$$

$$\Delta_2^{(i,j,k)} \widehat{f}_{(n)} = \begin{cases} B_1 \widehat{f}_{(n)}^{(i,j,k)} - B_2 \widehat{f}_{(n)}^{(i,j,k+1)} + B_3 \widehat{f}_{(n)}^{(i,j,k(i)) -}, & [\theta_\zeta^{(k+1)} < \text{Arcsin}(1/\widehat{r}^{(i)}) < \theta_\zeta^{(k+2)}], & (23c) \\ B_4 (\widehat{f}_{(n)}^{(i,j,k)} - \widehat{f}_{(n)}^{(i,j,k(i)) -}), & [\theta_\zeta^{(k)} < \text{Arcsin}(1/\widehat{r}^{(i)}) < \theta_\zeta^{(k+1)}], & (23d) \end{cases}$$

where

$$\widehat{f}_{(n)}^{(i(k),j,k)\pm} = \widehat{f}_{(n)}(1/\sin \theta_\zeta^{(k)} \pm 0, \zeta^{(j)}, \theta_\zeta^{(k)}), \quad (23e)$$

$$\widehat{f}_{(n)}^{(i,j,k(i)\pm} = \widehat{f}_{(n)}(\widehat{r}^{(i)}, \zeta^{(j)}, \text{Arcsin}(1/\widehat{r}^{(i)}) \pm 0), \quad (23f)$$

and the constants A_1 , A_2 , and A_3 (B_1 , B_2 , and B_3) are chosen in such a way that $\Delta_1^{(i,j,k)} \widehat{f}_{(n)}/(d\widehat{r}/di)$ [$\Delta_2^{(i,j,k)} \widehat{f}_{(n)}/(d\theta_\zeta/dk)$] is the difference expression of the second order accuracy for $\partial \widehat{f}_{(n)}/\partial \widehat{r}$ ($\partial \widehat{f}_{(n)}/\partial \theta_\zeta$) at $(\widehat{r}^{(i)}, \zeta^{(j)}, \theta_\zeta^{(k)})$; A_4 and B_4 give corresponding first order

formulae. A_1, \dots, A_4 and B_1, \dots, B_4 depend only on i and k . It is noted that $(i(k), j, k)$ and $(i, j, k(i))$ are not regular lattice points. The $i(k)$ and $k(i)$ represent the intersection of the characteristic $\hat{r} \sin \theta_\zeta = 1$ with the lattice lines $\theta_\zeta = \theta_\zeta^{(k)}$ and $\hat{r} = \hat{r}^{(i)}$ respectively. That is,

$$\left. \begin{aligned} \hat{r}^{(i(k))} &= 1/\sin \theta_\zeta^{(k)}, \\ \theta_\zeta^{(k(i))} &= \text{Arcsin}(1/\hat{r}^{(i)}). \end{aligned} \right\} \quad (24)$$

For a discontinuous function on the characteristic, the two limiting values as in Eqs. (23e) and (23f) should be considered. The formulae contain $\hat{f}_{(n)}^{(i(k),j,k)+}$ or $\hat{f}_{(n)}^{(i,j,k(i)) -}$, i.e., $\hat{f}_{(n)}$ on either side of the discontinuity. The sequence $\hat{f}_{(n)}^{(i,j,k(i))\pm}$ corresponding to $\hat{f}_{(n)}$ at $\hat{r}^{(i)}$ on each side of the discontinuity, is constructed by the following difference scheme:

$$\zeta^{(j)} \cos \theta_\zeta^{(k(i))} \Delta_1^{(i,j)\pm} \hat{f}_{(n)} = \frac{2}{\sqrt{\pi} K n_w} \hat{\rho}_{(n-1)}^{(i)} \left(\hat{f}_{e(n-1)}^{(i,j,k(i))} - \hat{f}_{(n)}^{(i,j,k(i))\pm} \right), \quad (25)$$

where $\Delta_1^{(i,j)\pm} \hat{f}_{(n)}$ corresponds to $\Delta_1^{(i,j,k)} \hat{f}_{(n)}$ ($0 \leq k \leq \widehat{K} - 1$) in Eqs. (22a) and (22b) with $\hat{f}_{(n)}^{(i,j,k)}$ replaced by $\hat{f}_{(n)}^{(i,j,k(i))\pm}$. The \pm sign is absent in $\hat{f}_{e(n-1)}^{(i,j,k(i))}$ since it is continuous.

Corresponding to the boundary condition (13), we impose the condition:

$$\hat{f}_{(n)}^{(0,j,k)} = \frac{2}{\sqrt{\pi}} \exp(-(\zeta^{(j)})^2), \quad (k = 0, 1, \dots, \widehat{K} - 1), \quad (26)$$

which is independent of k . As the condition at $\hat{r} = \hat{r}_D$, we assume

$$\hat{f}_{(n)}^{(I,j,k)} = 0, \quad (k = \widehat{K}, \dots, K), \quad (27a)$$

$$\hat{f}_{(n)}^{(I+1,j,k)} = 0, \quad (k = \widehat{K}, \dots, K). \quad (27b)$$

Two conditions are required since the second order difference scheme, Eq. (22c), is used in Eq. (21).

With these preparations of difference formulae, we construct the sequence $\hat{f}_{(n)}^{(i,j,k)}$ ($n = 0, 1, 2, \dots$) by the following process. Let $\hat{f}_{(n-1)}^{(i,j,k)}$, thus $\hat{\rho}_{(n-1)}^{(i)}$, $\hat{u}_{(n-1)}^{(i)}$, and $\hat{T}_{(n-1)}^{(i)}$, be known.⁴⁷

(i) For $\widehat{K} \leq k \leq K$, starting from $\hat{f}_{(n)}^{(I-1,j,k)}$, compute $\hat{f}_{(n)}^{(i,j,k)}$ using Eqs. (21), (22c), (22d), (27a), and (27b) in descending order of i down to $\hat{f}_{(n)}^{(0,j,k)}$. The step $i = i + 1$ to $i = i$ is as follows. Let $\hat{f}_{(n)}^{(i',j,k)}$ ($i' > i$) be given. Starting from $\hat{f}_{(n)}^{(i',j,K)}$, compute $\hat{f}_{(n)}^{(i',j,k)}$ using Eqs. (21), (22c), and (22d) [and Eqs. (27a) and (27b) for $i = I - 1, I - 2$] in descending order of k down to $\hat{f}_{(n)}^{(i',j,\widehat{K})}$. Carry out this step for every j .

(ii) Compute $\hat{f}_{(n)}^{(i,j,k(i))\pm}$ along the discontinuity using Eq. (25): $\hat{f}_{(n)}^{(i,j,k(i))+}$ is constructed from the initial data $\hat{f}_{(n)}^{(0,j,\widehat{K})}$ obtained in the preceding step (i),⁴⁸ $\hat{f}_{(n)}^{(i,j,k(i)) -}$ from the initial data determined by Eq. (13). The computation is continued until the discontinuity becomes negligibly small. Then, from a set of $\hat{f}_{(n)}^{(i,j,k(i))+}$, obtain $\hat{f}_{(n)}^{(i(k),j,k)+}$ by interpolation. [The data on the discontinuity in Eqs. (23a)–(23d) are now prepared.]

(iii) For $0 \leq k \leq \widehat{K} - 1$, the computation is carried out in ascending order of i , independently in the two regions $\hat{r} > 1/\sin \theta_\zeta$ and $\hat{r} < 1/\sin \theta_\zeta$ separated by the discontinuity. The step

$i = i - 1$ to $i = i$ is as follows. Let $\hat{f}_{(n)}^{(i',j,k)}$ ($i' < i$) be given. (a) For $\hat{r} > 1/\sin \theta_\zeta$, starting from $\hat{f}_{(n)}^{(i,j,\hat{K}-1)}$, compute $\hat{f}_{(n)}^{(i,j,k)}$ using Eqs. (21), (22a), (22d), (23a), (23b), and the data obtained in steps (i) and (ii) in descending order of k down to $\hat{f}_{(n)}^{(i,j,\hat{k})}$ where $\theta_\zeta^{(\hat{k}-1)} < \text{Arcsin}(1/\hat{r}^{(i)}) < \theta_\zeta^{(\hat{k})}$ (Ref. 49). (b) For $\hat{r} < 1/\sin \theta_\zeta$, starting from $\hat{f}_{(n)}^{(i,j,\hat{k}-1)}$, compute $\hat{f}_{(n)}^{(i,j,k)}$ using Eqs. (21), (22a), (22b), (22d), (23c), (23d), (26), and the data obtained in step (ii) in descending order of k down to $\hat{f}_{(n)}^{(i,j,0)}$. Carry out these steps for every j . For $i > i_c$, where the discontinuity is negligibly small, neglecting the discontinuity, compute $\hat{f}_{(n)}^{(i,j,k)}$ from $k = \hat{K} - 1$ to 0 only with the standard formulae (22a), (22b), and (22d) as in step (i). (iv) Applying the Simpson formula to Eqs. (12a)–(12c), compute $\hat{\rho}_{(n)}^{(i)}$, $\hat{u}_{(n)}^{(i)}$, and $\hat{T}_{(n)}^{(i)}$ from $\hat{f}_{(n)}^{(i,j,k)}$. (v) Repeat the process of (i)–(iv) with shift of the subscript (n to $n + 1$) until $\hat{f}_{(n)}^{(i,j,k)}$ converges. We take the limit as the solution $\hat{f}^{(i,j,k)}$.

The order of computation in the preceding process is consistent with the natural course of integration of Eq. (10) along its characteristics in the direction of molecular velocity.

IV. SOLUTIONS IN THE FREE MOLECULAR AND CONTINUUM LIMITS

Before presenting the result of the numerical analysis, we give the solutions of two extreme cases: the free molecular and the continuum limits. The general solution of a free molecular flow around a convex body is well-known.^{44,45,50} Thus, the solution of the present problem for $Kn_w = \infty$ is easily obtained as

$$\hat{f}(\hat{r}, \zeta, \theta_\zeta) = \begin{cases} \frac{2}{\sqrt{\pi}} \exp(-\zeta^2), & [0 \leq \theta_\zeta < \text{Arcsin}(1/\hat{r})], \\ 0, & [\text{Arcsin}(1/\hat{r}) < \theta_\zeta \leq \pi]. \end{cases} \quad (28a)$$

$$[\text{Arcsin}(1/\hat{r}) < \theta_\zeta \leq \pi]. \quad (28b)$$

At a given point in the gas, only the molecules whose velocities are inside the circular cone $\theta_\zeta < \text{Arcsin}(1/\hat{r})$ are present. The cone becomes more slender as the distance from the sphere increases. The height of \hat{f} is invariant with respect to the distance. From Eqs. (3a)–(3c), (4a), and (4b), the macroscopic variables ρ , u , T , T_\parallel , and T_\perp are given by

$$\rho/\rho_w = \frac{1}{2} \left(1 - \sqrt{1 - (L/r)^2} \right), \quad (29a)$$

$$u/(2RT_w)^{1/2} = \frac{1}{\sqrt{\pi}} \left(1 + \sqrt{1 - (L/r)^2} \right), \quad (29b)$$

$$T/T_w = 1 - \frac{2}{3\pi} \left(1 + \sqrt{1 - (L/r)^2} \right)^2, \quad (29c)$$

$$T_\parallel/T_w = \left(1 - \frac{2}{\pi} \right) \left(1 + \sqrt{1 - (L/r)^2} \right)^2 - \sqrt{1 - (L/r)^2}, \quad (29d)$$

$$T_\perp/T_w = \frac{1}{2} \left(1 + (L/r)^2 - \sqrt{1 - (L/r)^2} \right). \quad (29e)$$

The mass and energy fluxes Q and W are, from Eqs. (15) and (17),

$$Q/4\pi\rho_w(2RT_w)^{1/2}L^2 = \frac{1}{2\sqrt{\pi}}, \quad (30a)$$

$$W/4\pi p_w(2RT_w)^{1/2}L^2 = \frac{1}{\sqrt{\pi}}. \quad (30b)$$

The general behavior of steady flows of a slightly rarefied gas past its condensed phase, where (strong) evaporation or condensation is taking place, is studied in Ref. 26. In the limit of the Knudsen number being zero, the flow field is described by the solution of the Euler system of equations for an ideal gas under appropriate boundary conditions, with local corrections such as Knudsen layer^{22,25,32} or shock layer^{51,52}. According to Ref. 26 the boundary condition to be satisfied on the condensed phase at rest where evaporation is taking place is given as follows:

$$\frac{p}{p_w} = h_1(M), \quad \frac{T}{T_w} = h_2(M), \quad (M \leq 1), \quad (31)$$

where M is Mach number $(3u^2/5RT)^{1/2}$ and the numerical data of the functions of M , $h_1(M)$ and $h_2(M)$, for the BKW equation are shown in Table I. In addition, the tangential velocity should be zero. Thus, in the present problem with the spherical condensed phase, the conditions Eq. (31) among p , T , M , p_w , and T_w are applied at $r = L$.

The solution of the Euler system for the evaporating flow from a sphere into a vacuum is given by the following parametric expression in M :

$$\rho/\rho_* = 8/(3 + M^2)^{3/2}, \quad (32a)$$

$$u/(5RT_*/3)^{1/2} = 2M/(3 + M^2)^{1/2}, \quad (32b)$$

$$T/T_* = 4/(3 + M^2), \quad (32c)$$

$$r/L = (3 + M^2)/4M^{1/2}, \quad (32d)$$

where

$$\rho_* = h_1(1)\rho_w/h_2(1), \quad (32e)$$

$$T_* = h_2(1)T_w. \quad (32f)$$

Incidentally,

$$T_{\parallel} = T_{\perp} = T, \quad (32g)$$

since the Euler system corresponds to the local Maxwellian. For the BKW equation under the conventional boundary condition,

$$h_1(1)/h_2(1) = 0.3225, \quad h_2(1) = 0.6434. \quad (33)$$

The mass and energy fluxes Q and W from the sphere are given by

$$Q/4\pi\rho_w(2RT_w)^{1/2}L^2 = (5/6)^{1/2}h_1(1)/h_2(1)^{1/2}, \quad (34a)$$

$$W/4\pi p_w(2RT_w)^{1/2}L^2 = 4(5/6)^{3/2}h_1(1)h_2(1)^{1/2}. \quad (34b)$$

Thus, for the BKW equation,

$$Q/4\pi\rho_w(2RT_w)^{1/2}L^2 = 0.2361, \quad (35a)$$

$$W/4\pi p_w(2RT_w)^{1/2}L^2 = 0.5065. \quad (35b)$$

For large r/L , Eqs. (32a)–(32d) are reduced to

$$\rho/\rho_* = \frac{1}{2}(r/L)^{-2}, \quad (36a)$$

$$u/(5RT_*/3)^{1/2} = 2 - 3(4r/L)^{-4/3}, \quad (36b)$$

$$T/T_* = 4^{-1/3}(r/L)^{-4/3}, \quad (36c)$$

$$M = (4r/L)^{2/3}. \quad (36d)$$

There are two unclear points in this isentropic solution. The first point is that $d\rho/dr$, du/dr , etc. are infinite at $r = L$. This violates the assumption imposed in the derivation of the Euler system from the Boltzmann or BKW equation. The second point is the behavior of the solution for large r/L . The mean free path ℓ at the equilibrium at rest with ρ and T is

$$\ell = (8RT/\pi)^{1/2}/A_{col}\rho, \quad (37)$$

and the length scale L_r of variation ρ , u , etc. is $O[\rho(d\rho/dr)^{-1}]$. That is,

$$L_r = O(r). \quad (38)$$

The local Knudsen number Kn_r ($= \ell/L_r$) for large r/L increases with r as

$$Kn_r = O[Kn_w(r/L)^{1/3}]. \quad (39)$$

The local Knudsen number Kn_r , which characterizes the variation of the flow,⁵³ is not uniformly small for small Kn_w . It ranges from $O(Kn_w)$ to ∞ .

When Kn_w is very small, there is a region where Kn_r is small but M is large. Then, the isentropic solution is valid up to this region, with the reservation of the first unclear point raised in the preceding paragraph. The behavior downstream of this region can be studied by the hypersonic approximation, where a simplification is made under the assumption that the width of the velocity distribution function is much smaller than the flow speed (Refs. 35–38). According to Refs. 35 and 36, the solution of this approximation of a spherically expanding flow is expressed by the confluent hypergeometric functions as follows:

$$\hat{\rho} = c_0 \hat{r}^{-2}, \quad (40a)$$

$$\hat{u} = c_1, \quad (40b)$$

$$\hat{T} = \frac{1}{\hat{r}^2} [c_2 U(2/3, 3, \alpha/Kn_w \hat{r}) + c_3 M(2/3, 3, \alpha/Kn_w \hat{r})], \quad (40c)$$

$$\alpha = 2c_0/\sqrt{\pi}c_1,$$

where c_0 , c_1 , c_2 , and c_3 are undetermined constants, and $U(a, b, x)$ and $M(a, b, x)$ are Kummer's functions (of the same notation as in Ref. 54; don't confuse with Mach number M). The inner expansion (for $Kn_w \hat{r} \ll 1$)^{55,56} of the solution (40a)–(40c) is

$$\hat{\rho} = c_0 \hat{r}^{-2}, \quad (41a)$$

$$\hat{u} = c_1, \quad (41b)$$

$$\hat{T} = c_2 \left(\frac{Kn_w}{\alpha} \right)^{2/3} \frac{1}{\hat{r}^{4/3}} + c_3 \frac{2}{\Gamma(2/3)} \left(\frac{Kn_w}{\alpha} \right)^{7/3} \hat{r}^{1/3} \exp \left(\frac{\alpha}{Kn_w \hat{r}} \right), \quad (41c)$$

where $\Gamma(x)$ is the gamma function⁵⁴. Matching Eqs. (41a)–(41c) with the outer expansion, Eqs. (36a)–(36c), of the isentropic solution, we have⁵⁷

$$\left. \begin{aligned} c_0 &= h_1(1)/2h_2(1), & c_1 &= [10h_2(1)/3]^{1/2}, \\ c_2 &= [3h_1(1)^2/40\pi]^{1/3} Kn_w^{-2/3}, & c_3 &= 0. \end{aligned} \right\} \quad (42)$$

From Eqs. (40c) and (42), we have, for $r \rightarrow \infty$,

$$\left. \begin{aligned} T/T_w &\rightarrow A_0 Kn_w^{4/3}, \\ A_0 &= \left(\frac{5\pi}{3}\right)^{2/3} \frac{h_2(1)^3}{\Gamma(2/3)h_1(1)^{4/3}} = 4.828, \end{aligned} \right\} \quad (43)$$

which is the frozen temperature for small Kn_w . In this approximation the normal temperature T_{\perp} can be shown to decay as

$$\left. \begin{aligned} T_{\perp}/T_w &\rightarrow A_1 Kn_w^{1/3} L/r, \\ A_1 &= \left(\frac{5\pi}{24}\right)^{1/6} \frac{h_2(1)^{3/2}}{\Gamma(2/3)h_1(1)^{1/3}} = 0.5999, \end{aligned} \right\} \text{as } Kn_w(r/L) \rightarrow \infty. \quad (44)$$

V. RESULT AND DISCUSSION

A. Macroscopic variables

The distributions of the density, flow velocity, temperature, and Mach number, i.e., ρ/ρ_w , $u/(2RT_w)^{1/2}$, T/T_w , and $M [= u/(5RT/3)^{1/2}]$, are shown for various Knudsen numbers Kn_w in Figs. 1, 2, and Tables II–IV. Figure 1 shows the behavior near the sphere, and Fig. 2 shows the long range behavior. The data for $Kn_w = 0$ are the solution of the Euler system given by Eqs. (32a)–(32d). Their Knudsen-layer corrections, which flatten on $r/L = 1$, are also shown in the figures. In Fig. 2(c), the temperature profiles of the hypersonic approximation for small Kn_w are also shown by dashed lines. The reason of their deviation from the numerical solutions is given in connection with the behavior of the velocity distribution function. The data for $Kn_w = \infty$ are the free molecular solution given by Eqs. (29a)–(29c). The behavior of the gas varies very sharply near the sphere (Fig. 1) but approaches a vacuum state at infinity slowly (Fig. 2). The density vanishes as fast as $r^{-\alpha}$, where $\alpha = 2.00$ for all Knudsen numbers. The flow velocity and temperature approach nonzero values (except for T at $Kn_w = 0$), which depend on the Knudsen number. The limiting values $u_{\infty}/(2RT_w)^{1/2}$ and T_{∞}/T_w of $u/(2RT_w)^{1/2}$ and T/T_w as $r \rightarrow \infty$, the latter of which is called frozen temperature, are shown in Fig. 3 and Table V. These data were determined by close examination of the behavior of variation of ρ , u , and T for large r . The data $\ln \rho$, $\ln du/dr$, and $\ln dT/dr$ versus $\ln r$ are found to be linear, with high accuracy, for large r , from which the asymptotic forms of ρ , u , and T are determined. The $u_{\infty}/(2RT_w)^{1/2}$ and T_{∞}/T_w in Fig. 3 and Table V are the extrapolated values from the asymptotic forms. In Fig. 3, the frozen temperature (43) for small Kn_w obtained by the hypersonic approximation is also shown.

The profiles of parallel and normal temperatures T_{\parallel} and T_{\perp} [cf. Eqs. (4a) and (4b)] and their ratio T_{\perp}/T_{\parallel} , which are often referred to in experimental studies of nonequilibrium flows, are shown in Fig. 4. The parallel temperature T_{\parallel} for moderate and large Kn_w first decreases sharply and increases slowly to the value at infinity as r increases. This behavior is easily understood for the free molecular flow ($Kn_w = \infty$) by kinematic consideration. For the free molecular flow [Eqs. (28a), (28b)] the velocities of the molecules on the sphere range $0 \leq \xi_r < \infty$ ($0 \leq \theta_{\zeta} < \pi/2$) and their speeds are practically limited to a region of the order of $(2RT_w)^{1/2}$. With the distance from the sphere the molecules for $\text{Arcsin}(L/r) \leq \theta_{\zeta} \leq \pi/2$, where $\xi_r/(2RT_w)^{1/2}$ is small for small $(r/L - 1)$, disappears. Therefore the standard deviation of f with respect to ξ_r , which corresponds to T_{\parallel} , decreases for small $(r/L - 1)$. With the decrease of the molecules of the central part of ξ_r for moderate and large $(r/L - 1)$, the temperature T_{\parallel} increases in this region. For small Kn_w , on the other hand, the shrink of f with respect to ξ_t , or the decrease of T_{\perp} , with the distance from the sphere induces the decrease of T_{\parallel} owing to frequent molecular collisions. From Figs. 4(b) and 4(c), as $r \rightarrow \infty$,

$$T_{\perp} \rightarrow 0, \quad (45)$$

and the slopes of the curves T_{\perp} ($Kn_w \neq 0$ or ∞) in Figs. 4(b) and 4(c), corresponding to the speed of decay, approach -1 as $r \rightarrow \infty$ (Ref. 58), but the speed of convergence is much slower than that of the case of ρ in Fig. 2. The corresponding slopes for $Kn_w = 0$ and ∞ approach $-4/3$ and -2 respectively [Eqs. (29e), (32g), and (36c)]. From Eqs. (5) and (45),

$$T_{\parallel} \rightarrow 3T, \quad (\text{as } r \rightarrow \infty). \quad (46)$$

The ratio T_{\perp}/T_{\parallel} is a measure of anisotropy of the velocity distribution function around the flow velocity ($T_{\perp}/T_{\parallel} = 1$ when it is isotropic). Except for very small Knudsen numbers, the velocity distribution function shows strong anisotropy over the whole flow field (Fig. 4(d); see Sec. III C for more details).

B. Mass and energy fluxes

The nondimensional mass and energy fluxes $Q/4\pi\rho_w(2RT_w)^{1/2}L^2$ and $W/4\pi p_w(2RT_w)^{1/2}L^2$ (\widehat{Q} and \widehat{W} for short) versus the Knudsen number Kn_w are shown in Fig. 5 and Table V. They increase monotonically from the values at $Kn_w = 0$ [Eqs. (35a) and (35b)] to those at $Kn_w = \infty$ [Eqs. (30a) and (30b)]. The contributions to \widehat{Q} and \widehat{W} of the molecules leaving the sphere are equal to \widehat{Q} and \widehat{W} at $Kn_w = \infty$, respectively. Therefore, the differences from the free molecular values, which are negative, are the contributions of the molecules arriving on the sphere. For example, at $Kn_w = 0$, where $\widehat{Q}/\widehat{Q}(Kn_w = \infty) = 0.8370$ and $\widehat{W}/\widehat{W}(Kn_w = \infty) = 0.8977$, the 16.30% of the molecules leaving the sphere return to the sphere, but only 10.23% of the energy leaving the sphere return. This is because the returning molecules, on the average, have less energy than the leaving molecules.

The rate (16.30%) of the returning molecules at $Kn_w = 0$ is equal to that in the evaporating flow from a plane condensed phase that reaches sonic speed at infinity. This is obvious from the following structure of the isentropic solution [Eqs. (32a)–(32d)] of the evaporating flow from the sphere at $Kn_w = 0$. The boundary condition (31) for the Euler system corresponds to connection of an isentropic flow to an evaporating flow from a plane condensed phase.²⁶ The latter cannot be supersonic, but an isentropic expanding flow into a vacuum cannot be subsonic. Therefore, the connection of the two flows, which makes up the evaporating flow [Eqs. (32a)–(32d)] from the sphere, is made at sonic speed.

C. Velocity distribution function

The velocity distribution function $\hat{f} [= 2\pi\rho_w^{-1}(2RT_w)^{3/2}f]$ at several points in the gas, obtained by the numerical method in Sec. IV, are shown for $Kn_w = 0.01, 0.1, 1,$ and 10 in Figs. 6–11. The free molecular flow solution, Eqs. (28a) and (28b), is given in Fig. 12 for reference. At $Kn_w = \infty$, the molecular velocity is localized. That is, at a point (r), the molecules with velocity $0 \leq \theta_\zeta \leq \text{Arcsin}(L/r)$ come directly from the sphere and there are no molecules with the other velocity. The height of the velocity distribution function remains unchanged along the flow. At $Kn_w = 10$ (a large Knudsen number, Fig. 11), these features are well preserved and only local correction in (ξ_r, ξ_t) space is seen. The effect of collision is more eminent for smaller molecular speed because of smaller free path. The height of the distribution decreases only very slowly.

At $Kn_w = 0.01$ (Figs. 6 and 7), the behavior is quite different. The discontinuity of the velocity distribution function on the sphere decays in a very short distance (much shorter than the mean free path ℓ_w) [Fig. 6(a) \rightarrow Fig. 6(c)]. The distribution is transformed into a distribution fairly close to the Maxwellian distribution with the corresponding density, velocity, and temperature (the local Maxwellian f_e) in a distance of the several mean free paths [Fig. 6(a) \rightarrow Fig. 6(d) \rightarrow Fig. 7(a)]; see Figs. 13(a) and 14(a) for comparison with the local Maxwellian]. This is a kinetic transition process to a continuum region [Fig. 7(a)]. The transition region is the Knudsen layer and the region with discontinuity at the bottom of the Knudsen layer is the S layer, discussed in Refs. 34, 40, and 59. Along the flow, the density of the gas decreases and the collision effect becomes less important. Therefore the velocity distribution function begins to deviate from the Maxwellian, i.e., its width normal to the flow shrinks [Fig. 7(a) \rightarrow Fig. 7(b) \rightarrow Fig. 7(c)]. In this stage, the collision is still appreciable and the height of the distribution decreases considerably. Further away from the sphere, the density of the gas is so small that molecular collisions are rare. Thus, the flow is nearly free molecular and the height of the distribution decreases only very slowly [Fig. 7(c) \rightarrow Fig. 7(d)]. If the Mach number in the continuum region is sufficiently large, the downstream flow can be well expressed by the hypersonic approximation. In the present case ($Kn_w=0.01$), $M \sim 1.8$ in this region. This is not sufficiently large for the solution of the hypersonic approximation to be very good approximation at $Kn_w = 0.01$ or larger values as is seen in Fig. 2(c).

At $Kn_w = 0.1$, the discontinuity decays in the several mean free paths from the sphere [Fig. 8(a) \rightarrow Fig. 8(c)]. The distribution function there is of a shape with $T_\perp/T_\parallel < 1$ [Fig. 8(c); see Figs. 13(b) and 14(b) for comparison with the local Maxwellian], and this ratio decreases with the flow [Fig. 8(c) \rightarrow Fig. 9(a)]. That is, it is in a transition region that corresponds to the transition region in the downstream of the continuum region in the case $Kn_w = 0.01$. The behavior of further downstream is similar to the case $Kn_w = 0.01$, i.e., a transition region is followed by a free molecular region [Fig. 9(a) \rightarrow Fig. 9(b) \rightarrow Fig. 9(c)]. There is no continuum region in the flow. At $Kn_w = 1$, a transition region with large discontinuity [Fig. 10(a) \rightarrow Fig. 10(c)] is followed by a free molecular region with large discontinuity [Fig. 10(c) \rightarrow Fig. 10(d)].

In Fig. 15, $\delta = \rho^{-1} \iint |f - f_e| \xi_t d\xi_r d\xi_t$ versus r/L is shown for various Kn_w . If $f = f_e$, $\delta = 0$, and if f and f_e are disjoint, $\delta = 2$. The δ is a measure of deviation from the corresponding equilibrium distribution f_e . Figures 13(a) and 13(b), where comparison with the Maxwellian is made, are, respectively, the distributions marked with \bullet and \circ in Fig. 15. They are the points with nearly the smallest δ in the flows at $Kn_w = 0.01$ and 0.1 . From Fig. 15, the flow is seen to be highly nonequilibrium everywhere except for very small Knudsen numbers.

The transition to a free molecular flow region can clearly be seen from the profiles of \hat{f} at some ζ versus $\hat{r} \sin \theta_\zeta$ for various \hat{r} , which are shown in Fig. 16 for $Kn_w = 0.01, 0.2, 1,$ and 10 .

Since the characteristics of Eq. (10) are given by $\hat{r} \sin \theta_\zeta = \text{const}$, \hat{f} at a given ζ is expressed by a single curve if the flow is free molecular. The flow approaches a free molecular condition for large r/L even for $Kn_w = 0.01$. From Fig. 16 it is also seen that the discontinuity of the velocity distribution function remains appreciable at $r/L = 2000$ even for $Kn_w = 0.2$. By extrapolation it is found to be appreciable at downstream infinity. Since $A_{col}\rho$ is the collision frequency of a molecule, the integral $\int_{r_0}^{\infty} A_{col}\rho \xi_r^{-1} dr$ may be considered as the number of collision of a molecule with radial velocity ξ_r while it proceeds from r_0 to infinity.⁶⁰ The integral takes a finite value because $\rho \sim r^{-2}$ for large r . A molecule ($\xi_r \neq 0$) experiences only a finite number of collision before it reaches infinity. In other words, for large r_0 a molecule has rare chance of collision while proceeding from r_0 to infinity. This corresponds to our numerical results showing the free molecular behavior (resulting in the persistence of discontinuity) in the far field.

According to the free molecular feature of f (Fig. 16), the flow velocity and temperature are nearly constant (or their leading terms are constants that depend on Kn_w) in the far field (large r). On the other hand, T_\perp is proportional to (nearly) r^{-1} for $Kn_w \neq 0$ or ∞ but to r^{-2} for $Kn_w = \infty$ there [Figs. 4(b), 4(c), Eq. (44), and Eq. (29e)].⁶¹ This difference due to molecular collisions is a microstructure, and therefore more detailed consideration is required to understand this behavior. For large r , as we have seen, the width of the distribution f in the direction normal to the flow (or in ξ_t for short) is narrow. The gain term $A_{col}\rho f_e$ of the collision term in Eq. (1) has the same width in ξ_t as in ξ_r .⁶² Thus, the contribution of the gain term to the ξ_t -tail part of f is of the same order as that to the central part. The effect of molecular collisions relative to the local magnitude of f in ξ_t is much stronger on the tail. The contribution of the tail part to the normal temperature T_\perp is not negligible and plays an important role because the factor ξ_t^3 in Eq. (4b) significantly reduces the contribution of the central part of f . Thus, the effect of collisions is amplified and the difference appears.

D. Lattice system and accuracy tests

Since the behavior of the gas depends considerably on Kn_w , the lattice system [the lattice functions $\hat{r}(s)$, $\zeta(s)$, and $\theta_\zeta(s)$ defined in Eq. (19); I , J , K , and \widehat{K} ; \hat{r}_D and ζ_D] is chosen appropriately depending on Kn_w . Various tests have been carried out before the final computation. Here, the data of the lattice system that was used to obtain the results in Sec. V A, B, and C are summarized. (i) The lattice function $\hat{r}(s)$ is given by

$$\left. \begin{aligned} \frac{d\hat{r}}{ds} &= f_1(\hat{r})f_2(\hat{r}), & \hat{r}(0) &= 1, \\ f_1 &= d_2 + (d_1 - d_2)\exp(-d_3(\hat{r} - 1)), \\ f_2 &= 1 + (d_4 - 1)\exp(-d_5(\hat{r} - 1)), \end{aligned} \right\} \quad (47)$$

where d_1, d_2, \dots, d_5 are constants chosen properly in each case. The fundamental lattice moderately widening from the sphere is expressed by f_1 ; a finer lattice in the neighborhood of the sphere is expressed by f_2 . Examples of the lattice data are given in Table VI. The size \hat{r}_D of the \hat{r} domain is chosen as: $\hat{r}_D \sim 100$ for $Kn_w = 10$, $\hat{r}_D \sim 1000$ for $0.5 \leq Kn_w < 10$, and $\hat{r}_D \sim 2000$ for $Kn_w < 0.5$. (ii) For $\zeta^{(j)}$ lattice, $\zeta(s) = \alpha s^3$ (α : a constant), $\zeta_D = 8$, and $J = 192$ for $Kn_w < 0.1$ and $J = 96$ for $Kn_w \geq 0.1$. (iii) A fine lattice of θ_ζ is required near $\theta_\zeta = 0$ since \hat{f} is localized there for large \hat{r} . The number of the lattice points are chosen as: $(K, \widehat{K}) = (2560, 2464)$ for $Kn_w < 0.05$ and $(5760, 5568)$ for $Kn_w \geq 0.05$. Typical data of $\theta_\zeta^{(k)}$ are shown in Table VII.

Most of the lattice points are in $0 < \theta_\zeta < \pi/2$. (iv) The criterion of convergence of the sequence $\hat{f}_{(n)}^{(i,j,k)}$ is that the variations of the macroscopic variables $\hat{\rho}_{(n)}^{(i)}$, $\hat{u}_{(n)}^{(i)}$, and $\hat{T}_{(n)}^{(i)}$ over all lattice points on $1 \leq \hat{r} \leq \hat{r}_D$ in an iteration are less than 10^{-12} .

Here we summarize the accuracy test of our computation.

(i) The distribution function \hat{f} at $\zeta \geq 5.36$ ($\zeta_D = 8$) is bounded by 4×10^{-12} . Further, the differences of the macroscopic variables $\hat{\rho}$, \hat{u} , and \hat{T} for $\zeta_D = 8$ and $\zeta_D = 10.2$ at $Kn_w = 0.1$ are bounded by 2×10^{-14} over $1 \leq \hat{r} \leq \hat{r}_D$. Thus, the size $\zeta_D = 8$ adopted in our main computation may be considered sufficiently large.

(ii) Typical data of the maximum variations of the macroscopic variables $\hat{\rho}$, \hat{u} , and \hat{T} over the whole lattice points on $1 \leq \hat{r} \leq \hat{r}_D$ for different choices of \hat{r}_D are given in Table VIII. The variation of $\hat{\rho}$ is much smaller than the others in some cases. These data are also shown in the table. The $u_\infty/(2RT_w)^{1/2}$ and T_∞/T_w are extrapolated from the data of $|d\hat{u}/d\hat{r}|$ and $|d\hat{T}/d\hat{r}|$ for large \hat{r} . These data for different values \hat{r}_D are shown in Table IX.

(iii) Typical data of the maximum variations of $\hat{\rho}$, \hat{u} , and \hat{T} over the whole lattice points on $1 \leq \hat{r} \leq \hat{r}_D$ for different numbers J of the lattice points $\zeta^{(j)}$ are given in Table X. The maximum variation of $\hat{\rho}$ is shown separately when it is much smaller than that of the others.

(iv) Typical data of the maximum variation of $(\hat{\rho}, \hat{u}, \hat{T})$ over the whole lattice points on $1 \leq \hat{r} \leq \hat{r}_D$ for different numbers I and (K, \hat{K}) of the lattice points of (\hat{r}, θ_ζ) are shown in Fig. 17.

(v) The mass and energy fluxes Q and W are computed at all the lattice points $\hat{r}^{(i)}$ on $1 \leq \hat{r} \leq \hat{r}_D$, and the accuracies of the conservation relations (15) and (17) are examined. Their maximum variations $(Q_{\max} - Q_{\min})/Q_{\min}$ and $(W_{\max} - W_{\min})/W_{\min}$ are shown in Table XI. The $\hat{r}\theta_\zeta$ lattice dependence of these variations is shown in Fig. 17.

(vi) For the conservation relation (15) to hold with a given accuracy, $\hat{\rho}$ and \hat{u} should be computed with the same relative accuracy for all $\hat{r}^{(i)}$. Then, the absolute error of $\hat{\rho}$ for large \hat{r} should be very small since $\hat{\rho}$ tends to zero as $\hat{r} \rightarrow \infty$. The test (v) in Table XI suggests that the computation of $\hat{\rho}$ is very accurate for large \hat{r} . Typical examples of the variation of $\hat{\rho}$ at large \hat{r} in the tests corresponding to (ii), (iii), and (iv) are shown in Table XII for further evidence of the accuracy. The height of \hat{f} is almost invariant for large \hat{r} , and the domain where \hat{f} is appreciable shrinks as $\hat{r} \rightarrow \infty$ according as shrink of the view angle of the sphere. Thanks to this behavior of \hat{f} , with sufficient lattice points $\theta_\zeta^{(k)}$ in this region ($\theta_\zeta \sim 0$), we can compute \hat{f} without losing its relative accuracy much. Thus accurate $\hat{\rho}$ for large \hat{r} is obtained.

(vii) For some of Kn_w , the limiting solution $\hat{f}^{(i,j,k)}$ of the sequence $\hat{f}_{(n)}^{(i,j,k)}$ is examined to be independent of various choices of the initial function $\hat{f}_{(0)}^{(i,j,k)}$ of the iteration.

The computation was carried out by HP 9000 730 and MIPS RS 3230 computers at our laboratory.

VI. EFFECT OF CONDENSATION FACTOR IN KINETIC BOUNDARY CONDITION

As in most works on a gas flow with evaporation and condensation, we considered the problem under the conventional boundary condition [the assumption (ii) in Sec. II]. A generalization of the conventional boundary condition is reported in Ref. 12, where the effect of condensation factor is introduced and the conversion formula of the solution of the linearized half-space problem under the conventional condition to that under the generalized one is also given. The conversion relation is generalized to the two surface, the non linear half-space, and the cylindrical problems in Refs. 22, 26, 29, and 34. The generalized boundary condition introduced in

Ref. 12 is obtained by simply replacing the ρ_w in Eq. (7) by the following quantity:

$$\alpha_c \frac{p_w}{RT_w} - (1 - \alpha_c)(2\pi)^{3/2}(RT_w)^{-1/2} \iint_{\xi_r < 0} \xi_r \xi_t f d\xi_r d\xi_t, \quad (48)$$

where α_c is a constant ($0 \leq \alpha_c \leq 1$) called the condensation factor of the boundary. The case $\alpha_c = 1$ corresponds to the conventional condition. The two problems differ only in the boundary condition (6) by a factor. We can, therefore, derive a simple conversion formula between the two classes of solutions. Only the result is given here. Let the nondimensional solution ($\hat{f}, \hat{u}, \hat{\rho}, \hat{p}, \hat{T}, \hat{Q}$ $\{= Q/[4\pi\rho_w(2RT_w)^{1/2}L^2]\}$, \hat{W} $\{= W/[4\pi p_w(2RT_w)^{1/2}L^2]\}$) under the conventional boundary condition for $Kn_w = K_C$ be denoted by the subscript C , and let the solution under the generalized boundary condition for $Kn_w = K_G$ be denoted by the subscript G . The following one-to-one correspondence holds between the two classes of solutions:

$$(\hat{f}_G, K_G) = \Gamma(\hat{f}_C, K_C), \quad (49)$$

where

$$\Gamma = [1 + 2\sqrt{\pi}(1 - \alpha_c)\alpha_c^{-1}\hat{Q}_C]^{-1}. \quad (50)$$

Then,

$$(\hat{\rho}_G, \hat{p}_G, \hat{Q}_G, \hat{W}_G) = \Gamma(\hat{\rho}_C, \hat{p}_C, \hat{Q}_C, \hat{W}_C), \quad (51a)$$

$$(\hat{u}_G, \hat{T}_G, M_G) = (\hat{u}_C, \hat{T}_C, M_C). \quad (51b)$$

It is noted that all the ρ_w in Eqs. (9c), (9d), (11b), etc. [except in Eq. (7)] is the original ρ_w defined by $\rho_w = p_w/RT_w$ but not the quantity (48).

VII. CONCLUDING REMARKS

We have considered evaporating flows of a rarefied gas from its spherical condensed phase into a vacuum and analyzed the problem on the basis of the BKW equation numerically with a specially devised difference scheme capable of describing the discontinuity of the velocity distribution function. The velocity distribution function together with various important macroscopic variables is obtained accurately over the whole flow field for the entire range of the Knudsen number. The result is supplemented with an analytic solution for small Knudsen numbers, which is given by the solution of the Euler system of equations under the boundary condition (31) matched with the solution of hypersonic approximation for the far field. The distribution function shows strong anisotropy over the entire flow field even for small Knudsen numbers, and its discontinuity extends to downstream infinity for intermediate and large Knudsen numbers (and even for rather small Knudsen numbers). Even for $Kn_w = 0.1$, the velocity distribution function deviates considerably from the local Maxwellian distribution over the whole flow field. In most cases the velocity distribution function is far from an ellipsoidal distribution. The S layer at the bottom of the Knudsen layer are shown clearly. The velocity and temperature at downstream infinity take finite values, determined by the Knudsen number, except the temperature at zero Knudsen number. A simple formula deriving the solution for an arbitrary condensation factor in the kinetic boundary condition from that under the conventional boundary condition is also presented. In order to confirm the accuracy of computation, various tests are carried out. Especially, since the approach to the state at infinity is fairly slow, extensive tests are done by changing the size of the domain of \hat{r} and examining not only quantities under consideration themselves but also the rate of their variations.

REFERENCES

1. M. N. Kogan and N. K. Makashev, "Role of the Knudsen layer in the theory of heterogeneous reactions and in flows with surface reactions," *Fluid Dyn.* **6**, 913 (1971).
2. Y. P. Pao, "Application of kinetic theory to the problem of evaporation and condensation," *Phys. Fluids* **14**, 306, 1340 (1971).
3. C. E. Siewert and J. R. Thomas, Jr., "Half-space problems in the kinetic theory of gases," *Phys. Fluids* **16**, 1557 (1973).
4. Y. Sone and Y. Onishi, "Kinetic theory of evaporation and condensation," *J. Phys. Soc. Jpn.* **35**, 1773 (1973).
5. P. Gajewski, A. Kulicki, A. Wiśniewski, and M. Zgorelski, "Kinetic theory approach to the vapor-phase phenomena in a nonequilibrium condensation process," *Phys. Fluids* **17**, 321 (1974).
6. T. Matsushita, "Kinetic analysis of the problem of evaporation and condensation," *Phys. Fluids* **19**, 1712 (1976).
7. C. J. Knight, "Evaporation from a cylindrical surface into vacuum," *J. Fluid Mech.* **75**, 469 (1976).
8. Y. S. Lou, "On nonlinear droplet condensation and evaporation problem," *J. Appl. Phys.* **49**, 2350 (1978).
9. Y. Sone, "Kinetic theory of evaporation and condensation -Linear and nonlinear problems-," *J. Phys. Soc. Jpn.* **45**, 315 (1978).
10. Y. Sone and Y. Onishi, "Kinetic theory of evaporation and condensation -Hydrodynamic equation and slip boundary condition-," *J. Phys. Soc. Jpn.* **44**, 1981 (1978).
11. Y. Onishi and Y. Sone, "Kinetic theory of slightly strong evaporation and condensation -Hydrodynamic equation and slip boundary condition for finite Reynolds number-," *J. Phys. Soc. Jpn.* **47**, 1976 (1979).
12. J. W. Cipolla, Jr., H. Lang, and S. K. Loyalka, "Kinetic theory of condensation and evaporation. II," *J. Chem. Phys.* **61**, 69 (1974).
13. D. A. Labuntsov and A. P. Kryukov, "Analysis of intensive evaporation and condensation," *Int. J. Heat Mass Transfer* **22**, 989 (1979).
14. T. Ytrehus, "Theory and experiments on gas kinetics in evaporation," in *Rarefied Gas Dynamics*, edited by J. L. Potter (AIAA, New York, 1977), p. 1197.
15. S. M. Yen, "Numerical solutions of the Boltzmann and Krook equations for a condensation problem," in *Rarefied Gas Dynamics*, edited by S. S. Fisher (AIAA, New York, 1981), p. 356.
16. M. D. Arthur and C. Cercignani, "Non-existence of a steady rarefied supersonic flow in a half-space," *Z. Angew. Math. Phys.* **31**, 634 (1980).
17. A. A. Abramov and M. N. Kogan, "Conditions for supersonic condensation of gas," *Sov. Phys. Dokl.* **29**, 763 (1984).
18. A. P. Kryukov, "One-dimensional steady condensation of vapor velocities comparable to the velocity of sound," *Fluid Dyn.* **20**, 487 (1985).
19. Y. Sone, K. Aoki, and I. Yamashita, "A study of unsteady strong condensation on a plane condensed phase with special interest in formation of steady profile," in *Rarefied Gas Dynamics*, edited by V. C. Boffi and C. Cercignani (Teubner, Stuttgart, 1986), Vol. 2, p. 323.
20. Y. Sone and H. Sugimoto, "Strong evaporation from a plane condensed phase," *J. Vac. Soc. Jpn.* **31**, 420 (1988) (in Japanese).
21. H. Sugimoto and Y. Sone, "Strong evaporation from a plane condensed phase II," *J. Vac.*

- Soc. Jpn. **32**, 214 (1989) (in Japanese).
22. Y. Sone and H. Sugimoto, "Strong evaporation from a plane condensed phase," in *Adiabatic Waves in Liquid-Vapor Systems*, IUTAM Symposium, Göttingen, 1989, edited by G. E. A. Meier and P. A. Thompson (Springer, Berlin, 1990), p. 293.
 23. Y. Sone, K. Aoki, H. Sugimoto, and T. Yamada, "Steady evaporation and condensation on a plane condensed phase," *Theor. Appl. Mech. (Bulgaria)* **19**, No. 3, 89 (1988).
 24. Y. Sone, T. Ohwada, and K. Aoki, "Evaporation and condensation on a plane condensed phase - Numerical analysis of the linearized Boltzmann equation for hard-sphere molecules-," *Phys. Fluids A* **1**, 1398 (1989).
 25. K. Aoki, Y. Sone, and T. Yamada, "Numerical analysis of gas flows condensing on its plane condensed phase on the basis of kinetic theory," *Phys. Fluids A* **2**, 1867 (1990).
 26. K. Aoki and Y. Sone, "Gas flows around the condensed phase with strong evaporation or condensation - Fluid dynamic equation and its boundary condition on the interface and their application-," in *Advances in Kinetic Theory and Continuum Mechanics*, edited by R. Gatignol and Soubbaramayer (Springer, Berlin, 1991), p. 43.
 27. Y. Sone, "Asymptotic theory of a steady flow of a rarefied gas past bodies for small Knudsen numbers," in *Advances in Kinetic Theory and Continuum Mechanics*, edited by R. Gatignol and Soubbaramayer (Springer, Berlin, 1991), p. 19.
 28. Y. Sone, "Analytical and numerical studies of rarefied gas flows on the basis of the Boltzmann equation for hard-sphere molecules," in *Rarefied Gas Dynamics*, edited by A. E. Beylich (VCH, Weinheim, 1991), p. 489.
 29. Y. Sone, T. Ohwada, and K. Aoki, "Evaporation and condensation of a rarefied gas between its two parallel plane condensed phases with different temperatures and negative temperature-gradient phenomenon - Numerical analysis of the Boltzmann equation-," in *Mathematical Aspects of Fluid and Plasma Dynamics, Proceedings*, edited by G. Toscani, V. Boffi, and S. Rionero, Lecture Notes in Mathematics Vol. 1460 (Springer, Berlin, 1991), p. 186.
 30. M. N. Kogan and A. A. Abramov, "Direct simulation solution of the strong evaporation and condensation problem," in Ref.28, p. 1251.
 31. A. P. Kryukov, "Strong subsonic and supersonic condensation on a plane surface," in Ref.28, p. 1279.
 32. K. Aoki, K. Nishino, Y. Sone, and H. Sugimoto, "Numerical analysis of steady flows of a gas condensing on or evaporating from its plane condensed phase on the basis of kinetic theory: Effect of gas motion along the condensed phase," *Phys. Fluids A* **3**, 2260 (1991).
 33. D. Sibold and H. M. Urbassek, "Kinetic study of evaporation flows from cylindrical jets," *Phys. Fluids A* **3**, 870 (1991).
 34. H. Sugimoto and Y. Sone, "Numerical analysis of steady flows of a gas evaporating from its cylindrical condensed phase on the basis of kinetic theory," *Phys. Fluids A* **4**, 419 (1992).
 35. B. B. Hamel and D. R. Willis, "Kinetic theory of source flow expansion with application to free jet," *Phys. Fluids* **9**, 829 (1966).
 36. R. H. Edwards and H. K. Cheng, "Steady expansion of a gas into a vacuum," *AIAA J.* **4**, 558 (1966).
 37. N. C. Freeman, "Solution of the Boltzmann equation for expanding flows," *AIAA J.* **5**, 1696 (1967).
 38. R. E. Grundy, "Axially symmetric expansion of a monatomic gas from an orifice into a vacuum," *Phys. Fluids* **12**, 2011 (1969).
 39. Soubbaramayer, *Lecture Notes on Uranium Enrichment* (Tsinghua University, Peking, 1984) Fascicle 2.

40. Y. Sone and S. Takata, "Discontinuity of the velocity distribution function in a rarefied gas around a convex body and the S layer at the bottom of the Knudsen layer," *Transp. Theory Stat. Phys.* (to be published).
41. P. L. Bhatnagar, E. P. Gross, and M. Krook, "A model for collision processes in gases, I," *Phys. Rev.* **94**, 511 (1954).
42. P. Welander, "On the temperature jump in a rarefied gas," *Ark. Fys.* **7**, 507 (1954).
43. In the BKW equation the gain term $G(f)$ in the collision term $(G(f) - A_{col}\rho f)$ of the Boltzmann equation for pseudo Maxwell molecules is replaced by $A_{col}\rho f_e$. According to Kogan ("On the equations of motion of a rarefied gas," *J. Appl. Math. Mech.* **22**, 597 (1958)) the velocity distribution function of the molecules just collided, $G(f)$, is fairly close to $A_{col}\rho f_e$ even for a strongly nonisotropic f . Accordingly in the collision term $G(f) - A_{col}\rho f = [G(f) - A_{col}\rho f_e] + A_{col}\rho(f_e - f)$, the second term on the righthand side, where f_e differs greatly from f in highly nonequilibrium flows, is much larger than the first. Thus, the essential feature of nonequilibrium flow is well described by the BKW equation. Further, comparisons between Knudsen layer results for Boltzmann and BKW equations are given in Refs. 24 and 28.
44. M. N. Kogan, *Rarefied Gas Dynamics* (Plenum, New York, 1969), p. 401, Appendix 1.
45. This is a special feature of the BKW equation and the Boltzmann equation for hard-sphere molecules. For other molecular models, the problem contains another parameter U_0/mRT_w , where U_0 is the characteristic magnitude of the intermolecular potential and m is the mass of a molecule (Y. Sone, *Lecture Notes on Molecular Gas Dynamics*, Department of Aeronautical Engineering, Kyoto University, 1987).
46. F. Reif, *Fundamentals of Statistical and Thermal Physics* (McGraw-Hill, New York, 1965), p. 304.
47. Practically, only the data $\hat{\rho}_{(n-1)}^{(i)}$, $\hat{u}_{(n-1)}^{(i)}$, and $\hat{T}_{(n-1)}^{(i)}$ are used to obtain $\hat{f}_{(n)}^{(i,j,k)}$ in the present scheme for the BKW equation.
48. This means that $\hat{f}_{(n)}^{(0,j,\hat{K})}$ should be taken as the limiting value as $\theta_\zeta \rightarrow \pi/2 + 0$. The other limiting value is determined by Eq. (13).
49. In our lattice system, the characteristic $\hat{r} \sin \theta_\zeta = 1$ does not pass any lattice point $(\hat{r}^{(i)}, \theta_\zeta^{(k)})$.
50. C. Cercignani, *The Boltzmann Equation and Its Application* (Springer, Berlin, 1987) p. 262.
51. H. Grad, "Singular and nonuniform limits of solutions of the Boltzmann equation," in *Transport Theory*, edited by R. Bellman, G. Birkhoff, and I. Abu-Shumays (American Mathematical Society, Providence, RI, 1969), p. 269.
52. C. Cercignani and C. Lancellotti, "Velocity slip for curved shock waves," in *Rarefied Gas Dynamics*, edited by A. E. Beylich (VCH, Weinheim, 1991), p. 153.
53. In a hypersonic region, the mean free path based on the flow speed instead of the thermal speed characterizes the variation of the flow in its direction. With this mean free path, the effective Knudsen number is given by $Kn_r = O[Kn_w(r/L)]$. Incidentally, in a cylindrically expanding flow, $Kn_r = O(Kn_w)$ for the latter mean free path.
54. M. Abramowitz and I. A. Stegun, *Handbook of Mathematical Functions* (Dover, New York, 1968), p. 255, p. 504.
55. J. D. Cole, *Perturbation Method in Applied Mathematics* (Blaisdell Pub. Co., Mass., 1968) Chap. 1.
56. M. D. Van Dyke, *Perturbation Method in Fluid Mechanics* (Academic Press, New York, 1964) Chap. V.
57. From Eq. (42), α is $O(1)$ and positive, which is implicitly assumed in deriving Eq. (41c).
58. For $Kn_w = 10$, the data for larger r than shown in Fig. 4(c) are required.
59. Y. Sone, "New kind of boundary layer over a convex solid boundary in a rarefied gas," *Phys. Fluids* **16**, 1422 (1973).

60. We are not tracing a particular particle, but are simply considering the sum of the local expected number of collisions in dr . The change of ξ_r by collision should be taken into account in the former case.
61. Similar differences are seen in du/dr and dT/dr , which are determined by the second order terms of u and T for large r .
62. It is also true for a general molecular model that the width in ξ_t and in ξ_r of the distribution of the gain term of the collision integral are of the same order [see M. N. Kogan, "On the equation of motion of a rarefied gas", J. Appl. Math. Mech. **22**, 597 (1958)].

TABLE I. Functions $h_1(M)$ and $h_2(M)$ in Eq. (31).

M	h_1	h_2	M	h_1	h_2	M	h_1	h_2
0.0000	1.0000	1.0000	0.4000	0.4900	0.8470	0.8000	0.2695	0.7088
0.04999	0.9083	0.9798	0.4400	0.4593	0.8326	0.8400	0.2553	0.6956
0.07998	0.8582	0.9679	0.4800	0.4310	0.8184	0.8800	0.2420	0.6824
0.1200	0.7966	0.9521	0.5200	0.4050	0.8043	0.9200	0.2297	0.6693
0.1600	0.7404	0.9365	0.5600	0.3809	0.7904	0.9600	0.2182	0.6563
0.2000	0.6891	0.9212	0.6000	0.3586	0.7765	0.9700	0.2155	0.6530
0.2400	0.6421	0.9060	0.6400	0.3380	0.7628	0.9800	0.2128	0.6498
0.2800	0.5991	0.8910	0.6800	0.3189	0.7492	0.9900	0.2101	0.6466
0.3200	0.5596	0.8761	0.7200	0.3012	0.7356	1.0000	0.2075	0.6434
0.3600	0.5233	0.8615	0.7600	0.2848	0.7222			

TABLE II. The nondimensional density ρ/ρ_w versus r/L for various Knudsen numbers Kn_w .

r/L	ρ/ρ_w						
	$Kn_w = 0^a$	0.005	0.01	0.1	1	10	∞^b
1	0.3225	0.6143	0.6032	0.5427	0.5068	0.5007	0.5000
1.0001	0.3186	0.6002	0.5936	0.5368	0.5000	0.4936	0.4931
1.0002	0.3170	0.5908	0.5874	0.5339	0.4971	0.4908	0.4901
1.001	0.3099	0.5473	0.5565	0.5207	0.4849	0.4784	0.4777
1.002	0.3046	0.5154	0.5320	0.5100	0.4756	0.4692	0.4684
1.01	0.2820	0.4111	0.4397	0.4617	0.4364	0.4306	0.4298
1.02	0.2650	0.3581	0.3862	0.4252	0.4072	0.4021	0.4015
1.05	0.2318	0.2857	0.3075	0.3572	0.3515	0.3480	0.3475
1.1	0.1961	0.2290	0.2442	0.2908	0.2937	0.2920	0.2917
1.2	0.1514	0.1700	0.1792	0.2152	0.2237	0.2237	0.2236
1.4	0.1019	0.1114	0.1163	0.1393	0.1489	0.1500	0.1501
1.6	0.07433	0.08047	0.08365	0.09976	0.1082	0.1095	0.1097
1.8	0.05694	0.06129	0.06357	0.07562	0.08279	0.08410	0.08426
2	0.04513	0.04841	0.05013	0.05953	0.06561	0.06683	0.06699
5	0.06640	0.07040	0.07255	0.08572	0.09734	0.01006	0.01010
10	0.01631	0.01724	0.01775	0.02096	0.02402	0.02493	0.02506
20	4.05×10^{-4}	4.28×10^{-4}	4.40×10^{-4}	5.19×10^{-4}	5.98×10^{-4}	6.22×10^{-4}	6.25×10^{-4}
50	6.46×10^{-5}	6.81×10^{-5}	7.01×10^{-5}	8.27×10^{-5}	9.54×10^{-5}	9.94×10^{-5}	1.00×10^{-4}
100	1.61×10^{-5}	1.70×10^{-5}	1.75×10^{-5}	2.07×10^{-5}	2.38×10^{-5}	2.49×10^{-5c}	2.50×10^{-5}
200	4.03×10^{-6}	4.25×10^{-6}	4.37×10^{-6}	5.16×10^{-6}	5.96×10^{-6}	-	6.25×10^{-6}
1000	1.61×10^{-7}	1.70×10^{-7}	1.75×10^{-7}	2.06×10^{-7}	2.38×10^{-7}	-	2.50×10^{-7}
2000	4.03×10^{-8}	4.25×10^{-8}	4.37×10^{-8}	5.16×10^{-8}	-	-	6.25×10^{-8}

- a The isentropic solution (32a) and (32d). With the Knudsen-layer correction, which is flattened on the sphere, $\rho/\rho_w = 0.6362$ at $r/L = 1$.
- b The free molecular flow solution (29a).
- c The data at $r/L = 99.94$.

TABLE III. The nondimensional velocity $u/(2RT_w)^{1/2}$ versus r/L for various Knudsen numbers Kn_w .

r/L	$u/(2RT_w)^{1/2}$						
	$Kn_w = 0^a$	0.005	0.01	0.1	1	10	∞^b
1	0.7322	0.4011	0.4165	0.5017	0.5543	0.5631	0.5642
1.0001	0.7410	0.4105	0.4231	0.5072	0.5616	0.5711	0.5720
1.0002	0.7447	0.4169	0.4275	0.5098	0.5648	0.5742	0.5753
1.001	0.7605	0.4494	0.4505	0.5218	0.5781	0.5882	0.5894
1.002	0.7721	0.4763	0.4704	0.5317	0.5882	0.5985	0.5998
1.01	0.8208	0.5876	0.5601	0.5781	0.6310	0.6420	0.6434
1.02	0.8564	0.6614	0.6252	0.6156	0.6630	0.6739	0.6754
1.05	0.9242	0.7825	0.7411	0.6913	0.7249	0.7349	0.7362
1.1	0.9950	0.8896	0.8503	0.7740	0.7903	0.7981	0.7992
1.2	1.083	1.0071	0.9737	0.8789	0.8719	0.8754	0.8761
1.4	1.183	1.1285	1.1018	0.9975	0.9625	0.9593	0.9590
1.6	1.241	1.1964	1.1731	1.0661	1.0139	1.0055	1.0046
1.8	1.280	1.2410	1.2197	1.1114	1.0471	1.0348	1.0333
2	1.308	1.2728	1.2528	1.1436	1.0702	1.0547	1.0528
5	1.423	1.4004	1.3852	1.2706	1.1538	1.1215	1.1170
10	1.448	1.4292	1.4153	1.2988	1.1688	1.1310	1.1256
20	1.458	1.4408	1.4277	1.3106	1.1742	1.1335	1.1277
50	1.463	1.4466	1.4340	1.3168	1.1767	1.1344	1.1283
100	1.464	1.4483	1.4359	1.3187	1.1774	1.1346 ^c	1.1284
200	1.464	1.4491	1.4368	1.3196	1.1778	-	1.1284
1000	1.464	1.4497	1.4375	1.3204	1.1780	-	1.1284
2000	1.464	1.4497	1.4376	1.3205	-	-	1.1284

- a The isentropic solution (32b) and (32d). With the Knudsen-layer correction, which is flattened on the sphere, $u/(2RT_w)^{1/2} = 0.3712$ at $r/L = 1$.
b The free molecular flow solution (29b).
c The data at $r/L = 99.94$.

TABLE IV. The nondimensional temperature T/T_w versus r/L for various Knudsen numbers Kn_w .

r/L	T/T_w						
	$Kn_w = 0^a$	0.005	0.01	0.1	1	10	∞^b
1	0.6434	0.8257	0.8192	0.7912	0.7867	0.7876	0.7878
1.0001	0.6382	0.8215	0.8155	0.7863	0.7808	0.7815	0.7819
1.0002	0.6360	0.8189	0.8135	0.7841	0.7783	0.7791	0.7793
1.001	0.6265	0.8042	0.8031	0.7749	0.7676	0.7683	0.7684
1.002	0.6193	0.7908	0.7935	0.7678	0.7595	0.7600	0.7601
1.01	0.5884	0.7286	0.7448	0.7359	0.7241	0.7240	0.7240
1.02	0.5645	0.6838	0.7057	0.7102	0.6966	0.6959	0.6959
1.05	0.5162	0.6054	0.6307	0.6556	0.6405	0.6388	0.6387
1.1	0.4618	0.5298	0.5537	0.5913	0.5771	0.5744	0.5742
1.2	0.3886	0.4385	0.4583	0.5023	0.4920	0.4887	0.4883
1.4	0.2984	0.3334	0.3485	0.3921	0.3896	0.3872	0.3868
1.6	0.2419	0.2698	0.2823	0.3242	0.3283	0.3273	0.3272
1.8	0.2025	0.2261	0.2371	0.2781	0.2875	0.2881	0.2882
2	0.1734	0.1941	0.2042	0.2447	0.2588	0.2608	0.2611
5	0.04833	0.05810	0.06491	0.1114	0.1547	0.1666	0.1682
10	0.01895	0.02614	0.03220	0.08298	0.1376	0.1532	0.1554
20	0.00749	0.01333	0.01894	0.07184	0.1323	0.1497	0.1522
50	0.00220	0.00704	0.01228	0.06622	0.1301	0.1487	0.1513
100	8.73×10^{-4}	0.00527	0.01035	0.06455	0.1295	0.1485 ^c	0.1512
200	3.47×10^{-4}	0.00447	0.00946	0.06375	0.1293	-	0.1512
1000	4.05×10^{-5}	0.00389	0.00879	0.06314	0.1291	-	0.1512
2000	1.61×10^{-5}	0.00382	0.00871	0.06307	-	-	0.1512

- a The isentropic solution (32c) and (32d). With the Knudsen-layer correction, which is flattened on the sphere, $T/T_w = 0.8386$ at $r/L = 1$.
b The free molecular flow solution (29c).
c The data at $r/L = 99.94$.

TABLE V. Nondimensional velocity $u_\infty/(2RT_w)^{1/2}$ at infinity, frozen temperature T_∞/T_w , terminal Mach number $M_\infty [= u_\infty/(5RT_\infty/3)^{1/2}]$, mass flux $Q/4\pi\rho_w(2RT_w)^{1/2}L^2$, and energy flux $W/4\pi p_w(2RT_w)^{1/2}L^2$ for various Knudsen numbers Kn_w .

Kn_w	$u_\infty/(2RT_w)^{1/2}$	T_∞/T_w	M_∞	$Q/4\pi\rho_w(2RT_w)^{1/2}L^2$	$W/4\pi p_w(2RT_w)^{1/2}L^2$
0	1.464 ^a	0 ^b	∞	0.2361 ^c	0.5065 ^d
0.005	1.4499	0.0038	26	0.2465	0.5222
0.01	1.4377	0.0086	17	0.2512	0.5290
0.02	1.4162	0.0183	11.5	0.2573	0.5374
0.05	1.3686	0.0406	7.44	0.2663	0.5487
0.1	1.3206	0.0630	5.76	0.2723	0.5554
0.2	1.2700	0.0867	4.72	0.2765	0.5596
0.5	1.2108	0.1141	3.927	0.2793	0.5616
1	1.1781	0.1290	3.593	0.2806	0.5628
2	1.1564	0.1388	3.400	0.2813	0.5634
5	1.1407	0.1458	3.273	0.2817	0.5637
10	1.1347	0.1484	3.227	0.2819	0.5640
∞	1.1284 ^e	0.1512 ^f	3.179	0.2821 ^g	0.5642 ^h

- a From Eqs. (32b) and (32d).
- b From Eqs. (32c) and (32d).
- c Eq. (35a).
- d Eq. (35b).
- e From Eq. (29b).
- f From Eq. (29c).
- g Eq. (30a).
- h Eq. (30b).

TABLE VI. Typical data of the lattice of \bar{r} .

$Kn_w = 0.01$			0.1			1			10		
i	$\bar{r}^{(i)}$	$d\bar{r}/di$	i	$\bar{r}^{(i)}$	$d\bar{r}/di$	i	$\bar{r}^{(i)}$	$d\bar{r}/di$	i	$\bar{r}^{(i)}$	$d\bar{r}/di$
0	1	6.250×10^{-9}	0	1	1.563×10^{-7}	0	1	3.125×10^{-6}	0	1	6.250×10^{-5}
277	1.001	2.677×10^{-5}	523	1.001	6.858×10^{-6}	-	-	-	-	-	-
397	1.010	1.241×10^{-4}	1000	1.010	3.103×10^{-5}	767	1.010	3.434×10^{-5}	-	-	-
669	1.099	6.833×10^{-4}	2091	1.100	1.717×10^{-4}	1476	1.100	3.148×10^{-4}	383	1.100	6.847×10^{-4}
915	1.499	3.179×10^{-3}	3073	1.500	7.962×10^{-4}	1989	1.500	1.564×10^{-3}	629	1.500	3.186×10^{-3}
1245	4.988	2.496×10^{-2}	4394	5.001	6.261×10^{-3}	2654	4.997	1.249×10^{-2}	959	4.999	2.506×10^{-2}
1762	99.80	0.6025	6462	100.1	0.1511	3682	100.1	0.3089	1472	99.94	0.6183
2328	2018	7.940	8720	2010	1.981	4432	1010	3.075	-	-	-
	($= \bar{r}_D$)			($= \bar{r}_D$)			($= \bar{r}_D$)			($= \bar{r}_D$)	

TABLE VII. Typical data of the lattice of θ_ζ .

$Kn_w < 0.05$			$Kn_w \geq 0.05$		
k	$\theta_\zeta^{(k)}$	$d\theta_\zeta/dk$	k	$\theta_\zeta^{(k)}$	$d\theta_\zeta/dk$
0	0	1.750×10^{-5}	0	0	3.734×10^{-6}
57	1.005×10^{-3}	1.788×10^{-5}	253	1.000×10^{-3}	4.393×10^{-6}
412	1.001×10^{-2}	3.811×10^{-5}	1172	1.001×10^{-2}	1.836×10^{-5}
1208	0.1000	2.310×10^{-4}	2837	0.1000	1.077×10^{-4}
2200	0.7845	1.715×10^{-3}	4995	0.7848	7.853×10^{-4}
2464	$\pi/2$	5.698×10^{-3}	5568	$\pi/2$	2.663×10^{-3}
2560	π	8.608×10^{-2}	5760	π	7.966×10^{-2}
	(K, \bar{K}) = (2560, 2464)			(5760, 5568)	

TABLE VIII. The maximum variation of $\hat{\rho}$, \hat{u} , and \hat{T} over the whole lattice points on $1 \leq f \leq \bar{f}_D$ for different choices of \bar{f}_D . The maximum variation of $\hat{\rho}$ is shown in the parentheses when it is much smaller than that of the others. The value with *, smaller than 10^{-12} , means only that they are sufficiently small since they are smaller than the criterion of the convergence of the sequence $\hat{f}_{(i,j,k)}^{(\zeta)}$ (see the first paragraph in Sec. V D).

$K\bar{n}_w$	0.01	0.1	1	10
I (\bar{f}_D) ^a	$7 \times 10^{-13*}$	10^{-14*}	10^{-8}	10^{-8}
II (\bar{f}_D) ^b	$8 \times 10^{-13*}$	$2 \times 10^{-14*}$	6×10^{-9}	5×10^{-9}
			$(2 \times 10^{-13*})$	$(2 \times 10^{-13*})$
			$(3 \times 10^{-14*})$	$(3 \times 10^{-14*})$

- a I (\bar{f}_D): Comparison between the cases $\bar{f}_D \sim 100$ and 1000 ($K\bar{n}_w = 0.01$ and 0.1), $\bar{f}_D \sim 100$ and 200 ($K\bar{n}_w = 1$ and 10).
- b II (\bar{f}_D): Comparison between the cases $\bar{f}_D \sim 1000$ and 2000 ($K\bar{n}_w = 0.01$ and 0.1), $\bar{f}_D \sim 200$ and 1000 ($K\bar{n}_w = 1$ and 10).

TABLE IX. The comparison of $u_{\infty}/(2RT_w)^{1/2}$ and T_{∞}/T_w for different choices of \bar{f}_D . The upper line in each row is $u_{\infty}/(2RT_w)^{1/2}$ and the lower is T_{∞}/T_w . The data in the parentheses are $u/(2RT_w)^{1/2}$ and T/T_w at $\bar{f} = \bar{f}_D$.

$K\bar{n}_w$	0.01	0.1	1	10
$\bar{f}_D \sim 100$ ^{a,b}	1.4375 (1.4360)	1.3204 (1.3188)	1.1780 (1.1774)	1.1347 (1.1346)
	0.0088 (0.0103)	0.0632 (0.0645)	0.1291 (0.1295)	0.1484 (0.1485)
$\bar{f}_D \sim 200$ ^c			1.1781 (1.1777)	1.1347 (1.1347)
			0.1291 (0.1291)	0.1484 (0.1484)
$\bar{f}_D \sim 1000$ ^d	1.4377 (1.4375)	1.3206 (1.3204)	1.1781 (1.1780)	1.1347 (1.1347)
	0.0086 (0.0088)	0.0630 (0.0631)	0.1290 (0.1291)	0.1484 (0.1484)
$\bar{f}_D \sim 2000$ ^e	1.4377 (1.4376)	1.3206 (1.3205)		
	0.0086 (0.0087)	0.0630 (0.0631)		

- a The value of \bar{f}_D is approximate since the lattice points are not common to all $K\bar{n}_w$.
- b The values of $u_{\infty}/(2RT_w)^{1/2}$ and T_{∞}/T_w in this row are extrapolated from the data on $10 < \bar{f} < \bar{f}_D$.
- c Extrapolated from the data on $20 < \bar{f} < \bar{f}_D$.
- d Extrapolated from the data on $100 < \bar{f} < \bar{f}_D$.
- e Extrapolated from the data on $200 < \bar{f} < \bar{f}_D$.

TABLE X. The maximum variation of $\hat{\rho}$, \hat{u} , and \hat{T} over the whole lattice points on $1 \leq \bar{f} \leq \bar{f}_D$ for different numbers J of the lattice points of ζ . The maximum variation $\hat{\rho}$ is shown in the parentheses when it is much smaller than that of the others. The value with *, smaller than 10^{-12} , means only that they are sufficiently small since they are smaller than the criterion of the convergence of the sequence $\hat{f}_{(i,j,k)}^{(\zeta)}$ (see the first paragraph in Sec. V D).

$K\bar{n}_w$	0.01	0.1	1	10
I ($\zeta^{(j)}$) ^a		5×10^{-5}		
		(6×10^{-8})		
II ($\zeta^{(j)}$) ^b	7×10^{-4}	10^{-10}	4×10^{-11}	10^{-10}
	(3×10^{-8})	$(8 \times 10^{-13*})$		
III ($\zeta^{(j)}$) ^c	6×10^{-9}			
	$(2 \times 10^{-13*})$			

- a I ($\zeta^{(j)}$): Comparison between the cases $J = 46$ and 96 .
- b II ($\zeta^{(j)}$): Comparison between the cases $J = 96$ and 192 .
- c III ($\zeta^{(j)}$): Comparison between the cases $J = 192$ and 384 .

TABLE XI. The maximum variations of Q and W for different positions of their computation on $1 \leq \bar{f} \leq \bar{f}_D$.

$K\bar{n}_w$	0.01	0.1	1	10
$(Q_{\max} - Q_{\min})/Q_{\min}$	0.0003	0.0002	0.001	0.0003
$(W_{\max} - W_{\min})/W_{\min}$	0.0003	0.0002	0.001	0.0002

TABLE XII. The maximum variation of $\hat{\rho}$ at large \bar{f} in the tests in Tables VIII, X, and Fig. 17. The value with *, smaller than 10^{-12} , means only that they are very small since they are smaller than the criterion of the convergence of the sequence $\hat{f}_{(i,j,k)}^{(\zeta)}$ (see the first paragraph in Sec. V D).

$K\bar{n}_w$	0.01	0.1	1	10
II (\bar{f}_D) ^a	10^{-17*}	$3 \times 10^{-19*}$	$3 \times 10^{-15*}$	$3 \times 10^{-14*}$
II ($\zeta^{(j)}$) ^b	8×10^{-9}	$3 \times 10^{-16*}$	$4 \times 10^{-14*}$	$3 \times 10^{-13*}$
III (\bar{f}_D) ^c	3×10^{-9}	10^{-10}	9×10^{-8}	3×10^{-8}

- a The maximum variation of $\hat{\rho}$ over the whole lattice points on $\bar{f}_D \geq \bar{f} \geq 200$ ($K\bar{n}_w = 0.01$ and 0.1) and $\bar{f}_D \geq \bar{f} \geq 50$ ($K\bar{n}_w = 1$ and 10) in the test II (\bar{f}_D) in Table VIII.
- b The maximum variation of $\hat{\rho}$ over the whole lattice points on $\bar{f}_D \geq \bar{f} \geq 200$ ($K\bar{n}_w = 0.01$ and 0.1) and $\bar{f}_D \geq \bar{f} \geq 50$ ($K\bar{n}_w = 1$ and 10) in the test II ($\zeta^{(j)}$) in Table X.
- c The maximum variation of $\hat{\rho}$ over the whole lattice points on $\bar{f}_D \geq \bar{f} \geq 200$ ($K\bar{n}_w = 0.01$ and 0.1) and $\bar{f}_D \geq \bar{f} \geq 50$ ($K\bar{n}_w = 1$ and 10) in the test II in Fig. 17.

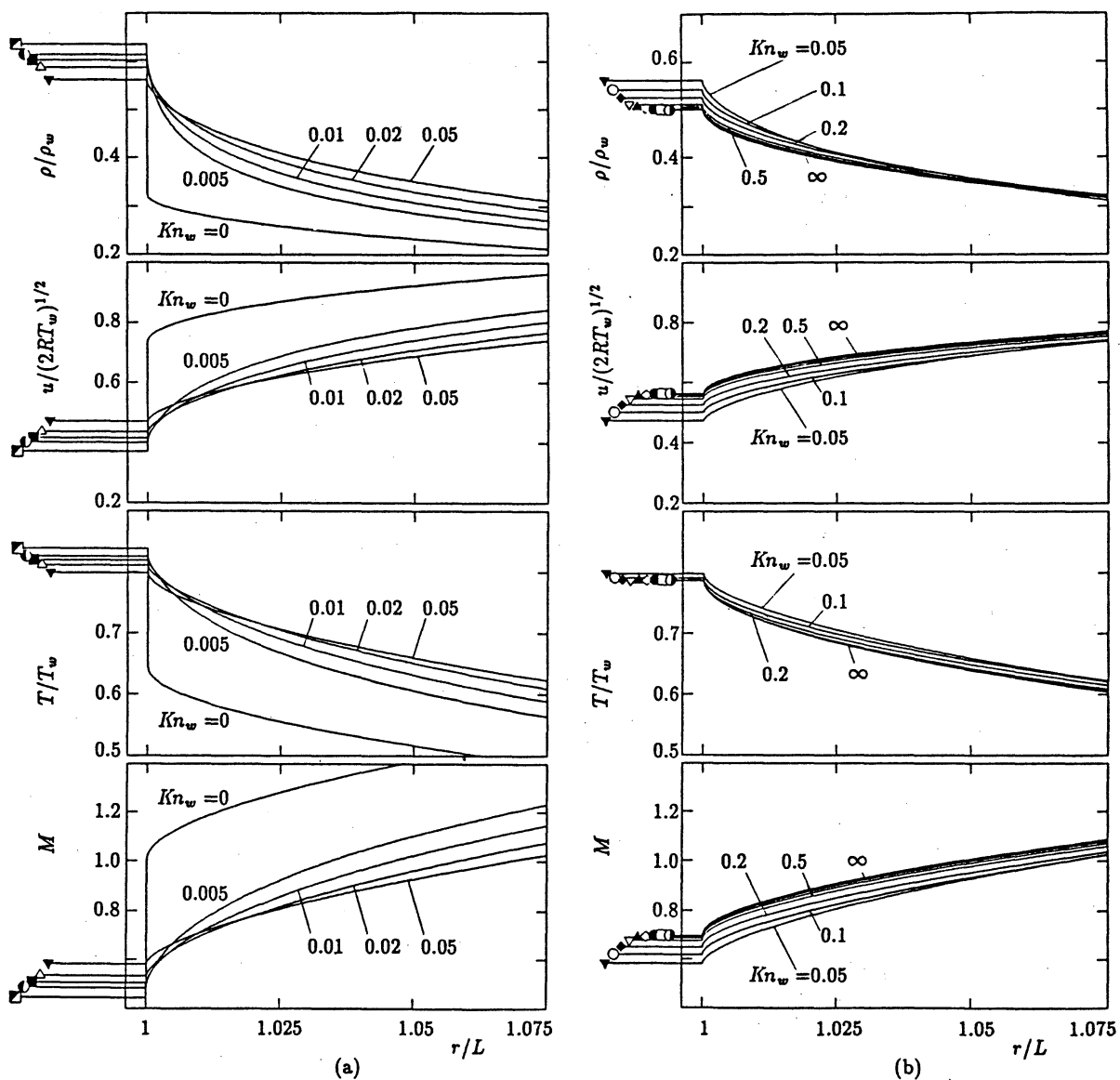


FIG. 1. The profiles of the macroscopic variables ρ/ρ_w , $u/(2RT_w)^{1/2}$, T/T_w , and M in the neighborhood of the sphere for various Knudsen numbers Kn_w . (a) $Kn_w = 0-0.05$ and (b) $0.05-\infty$. The value on the sphere are marked with \blacksquare for $Kn_w = 0$, \bullet for 0.005, \blacksquare for 0.01, \triangle for 0.02, \blacktriangledown for 0.05, \circ for 0.1, \blacklozenge for 0.2, ∇ for 0.5, \blacktriangle for 1, \diamond for 2, \bullet for 5, \square for 10, and \odot for ∞ .

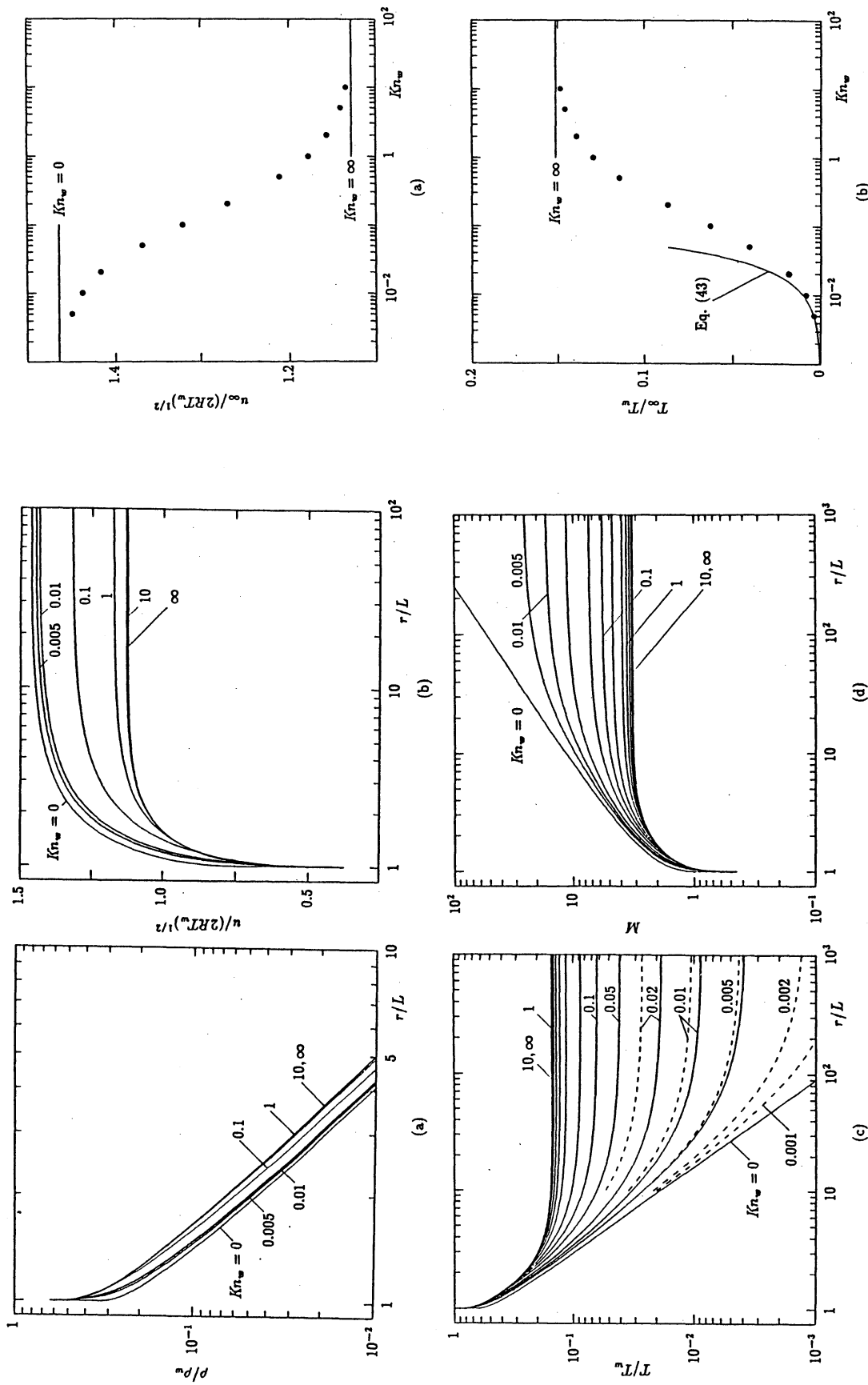


FIG. 2. The overall profiles of the macroscopic variables ρ/ρ_w , $u/(2RT_w)^{1/2}$, T/T_w , and M for various Knudsen numbers Kn_w . (a) ρ/ρ_w for $Kn_w = 0, 0.005, 0.01, 0.1, 1, 10$, and ∞ . (b) T/T_w for $Kn_w = 0, 0.005, 0.01, 0.1, 1, 10$, and ∞ . (c) T/T_w for $Kn_w = 0, 0.005, 0.01, 0.02, 0.05, 0.1, 0.2, 0.5, 1, 2, 5, 10$, and ∞ . The dashed line indicates the hypersonic approximation, Eq. (40c) with Eq. (42). (d) M [$= u/(5RT/3)^{1/2}$] for $Kn_w = 0, 0.005, 0.01, 0.02, 0.05, 0.1, 0.2, 0.5, 1, 2, 5, 10$, and ∞ .

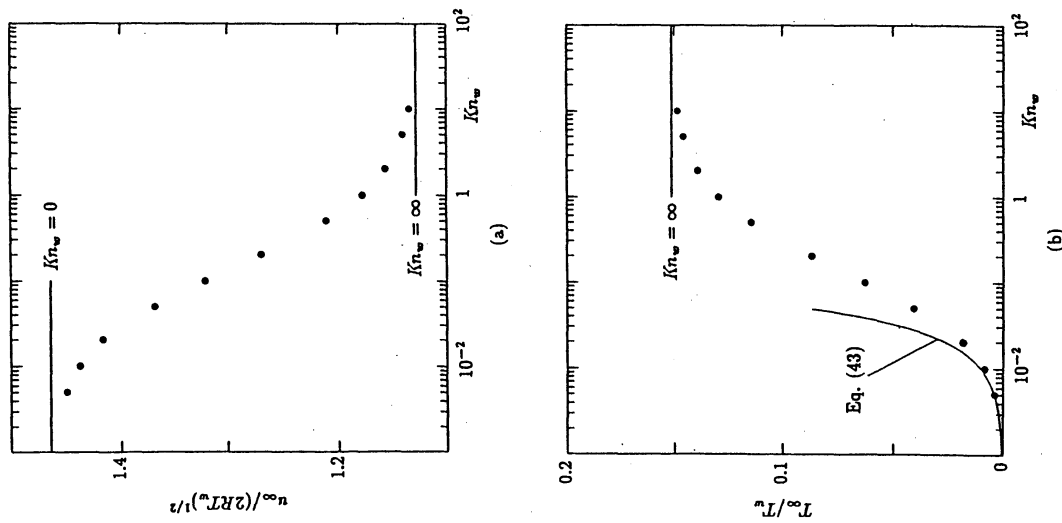


FIG. 3. The nondimensional flow velocity $[u_\infty/(2RT_w)^{1/2}]$ and temperature T_∞/T_w (frozen temperature) at infinity versus the Knudsen number Kn_w . (a) $u_\infty/(2RT_w)^{1/2}$ and (b) T_∞/T_w .

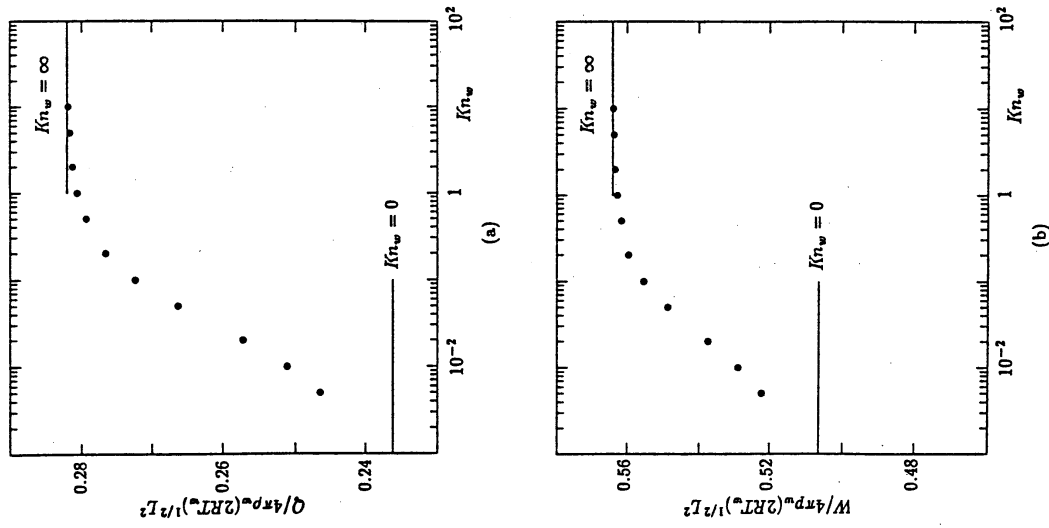


FIG. 5. The nondimensional mass flux $Q/4\pi\rho_w(2RT_w)^{1/2}L^2$ and the nondimensional energy flux $W/4\pi\rho_w(2RT_w)^{1/2}L^2$ from the sphere versus the Knudsen number Kn_w . (a) $Q/4\pi\rho_w(2RT_w)^{1/2}L^2$ and (b) $W/4\pi\rho_w(2RT_w)^{1/2}L^2$.

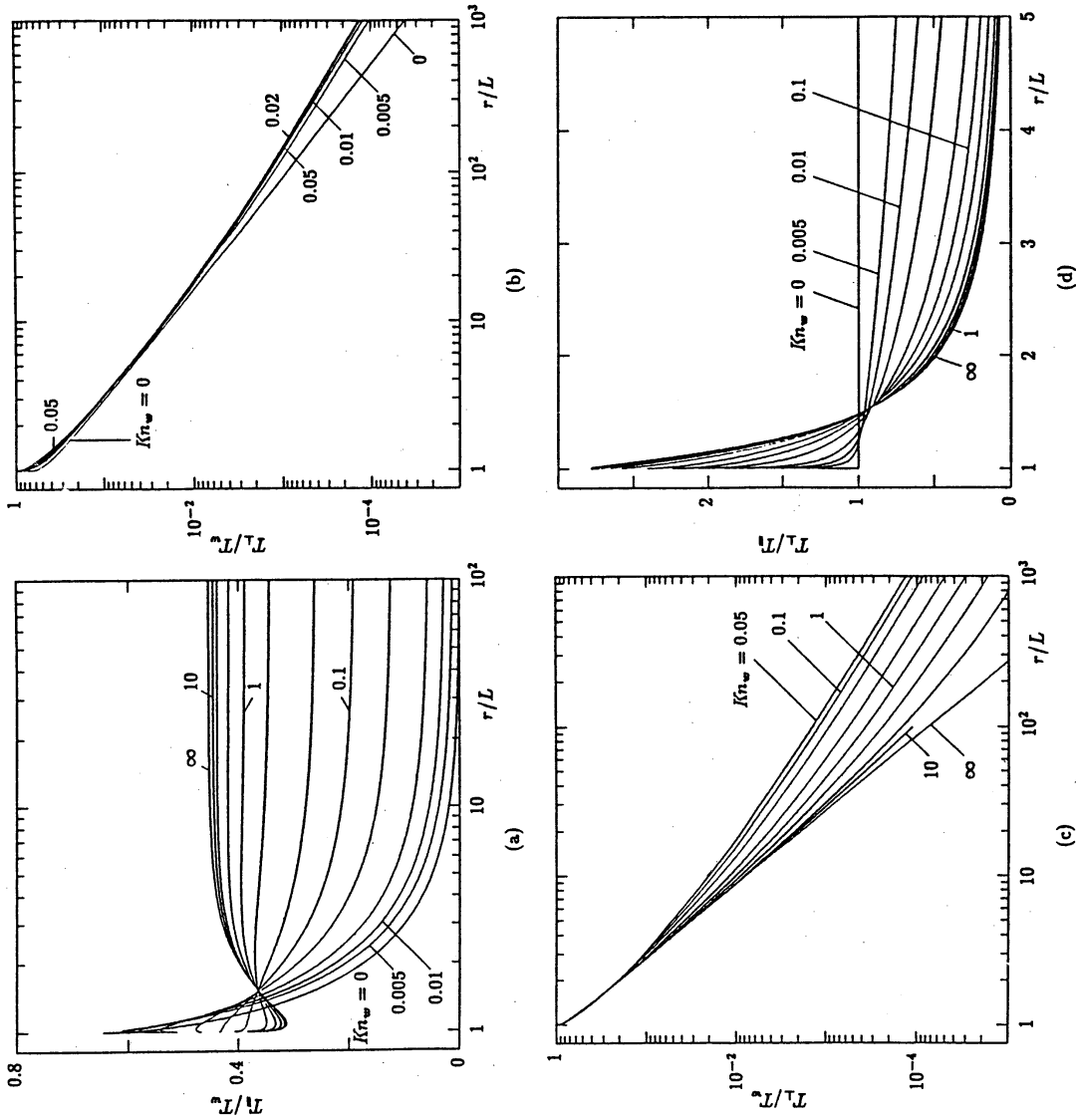


FIG. 4. The parallel and normal temperatures $T_{||}$ and T_{\perp} versus r . (a) $T_{||}/T_w$ for $Kn_w = 0, 0.005, 0.01, 0.02, 0.05, 0.1, 0.2, 0.5, 1, 2, 5, 10,$ and ∞ ; (b) T_{\perp}/T_w for $Kn_w = 0, 0.005, 0.01, 0.02, 0.05$; (c) $T_{||}/T_w$ for $Kn_w = 0.05, 0.1, 0.2, 0.5, 1, 2, 5, 10,$ and ∞ ; and (d) T_{\perp}/T_w for $Kn_w = 0, 0.005, 0.01, 0.02, 0.05, 0.1, 0.2, 0.5, 1, 2, 5, 10,$ and ∞ .

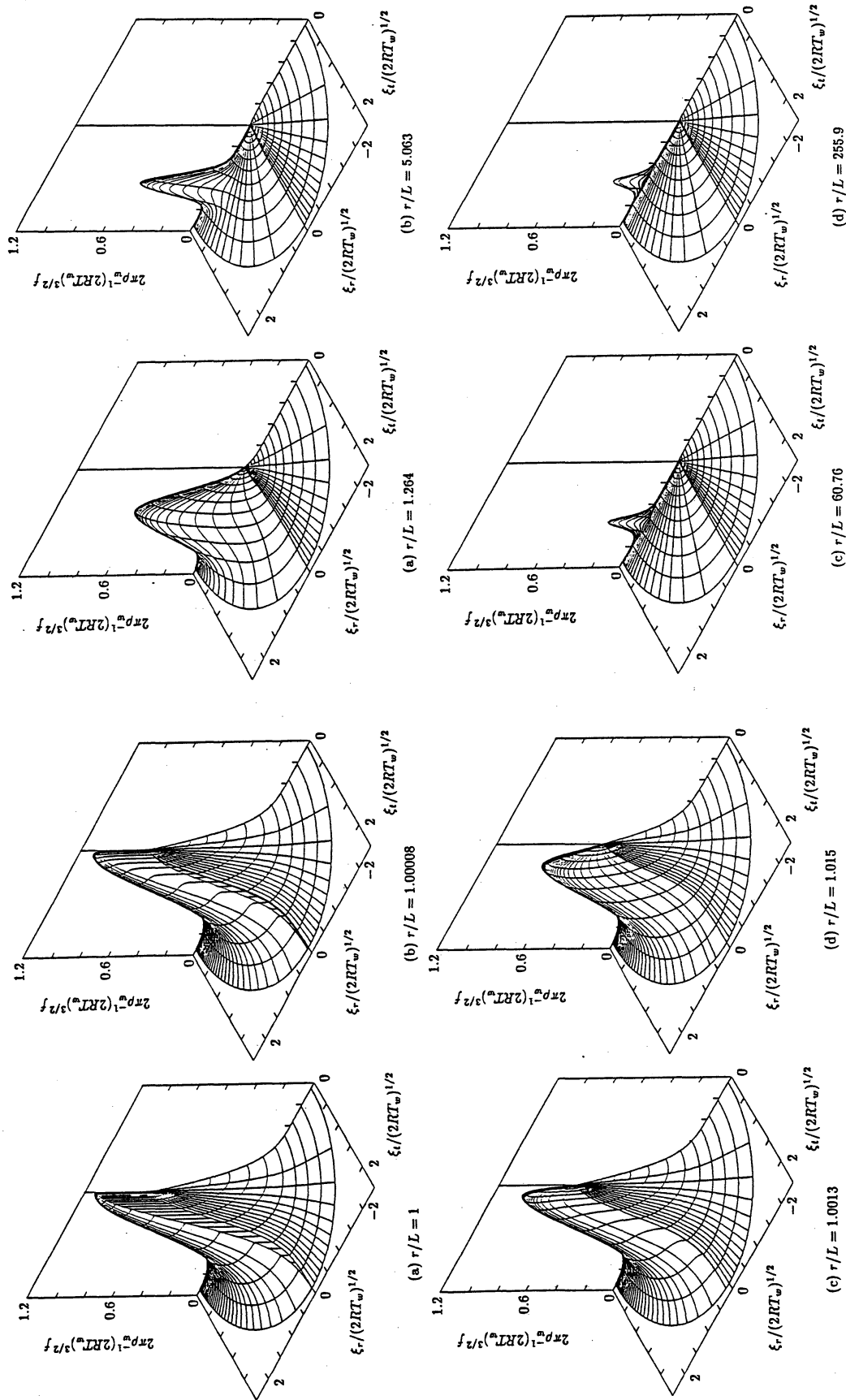
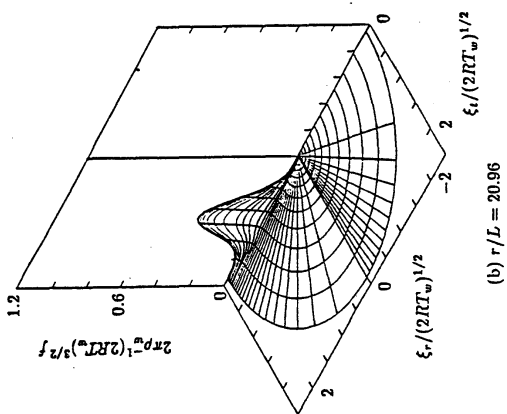
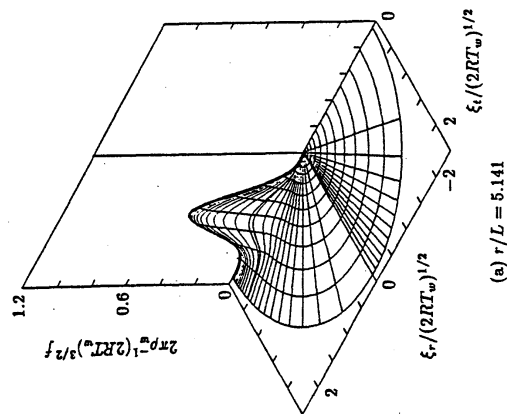


FIG. 6. The nondimensional velocity distribution function $2\pi\rho_w^{-1}(2RT_w)^{3/2}f$ at $Kn_w = 0.01$ (I): the S and Knudsen layers. (a) $r/L = 1$, (b) $r/L = 1.00008$, (c) $r/L = 1.0013$, and (d) $r/L = 1.015$.

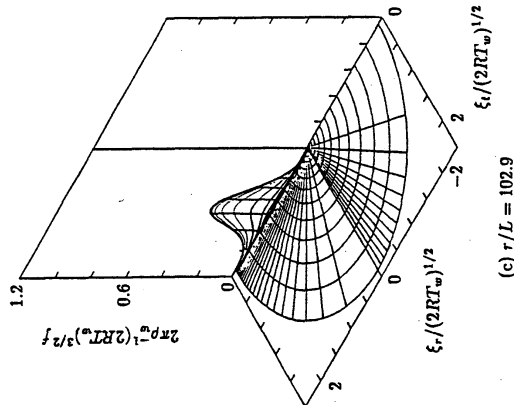
FIG. 7. The nondimensional velocity distribution function $2\pi\rho_w^{-1}(2RT_w)^{3/2}f$ at $Kn_w = 0.01$ (II): the continuum, transition, and free molecular regions. (a) $r/L = 1.264$, (b) $r/L = 5.063$, (c) $r/L = 60.70$, and (d) $r/L = 255.9$.



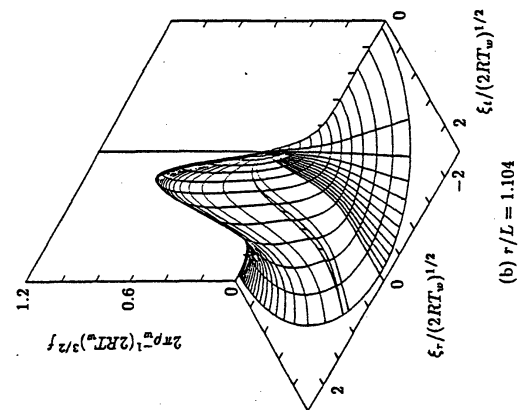
(b) $r/L = 20.96$



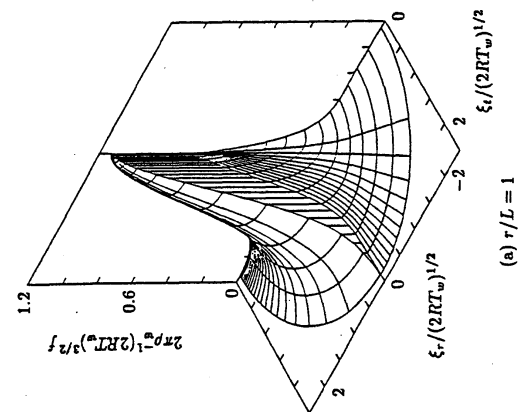
(a) $r/L = 5.141$



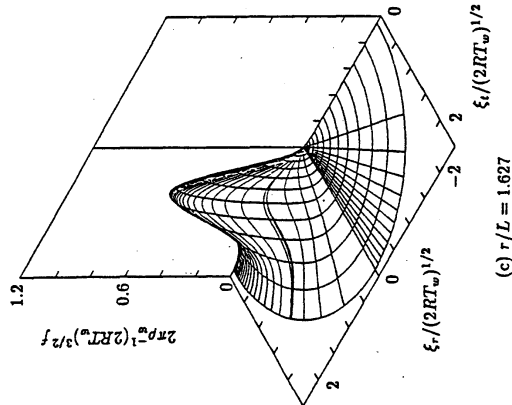
(c) $r/L = 102.9$



(b) $r/L = 1.104$



(a) $r/L = 1$



(c) $r/L = 1.627$

FIG. 8. The nondimensional velocity distribution function $2\pi\rho_w^{-1}(2RT_w)^{3/2}f$ at $Kn_w = 0.1$ (I); decay of the discontinuity in the transition region. (a) $r/L = 1$, (b) $r/L = 1.104$, and (c) $r/L = 1.627$.

FIG. 9. The nondimensional velocity distribution function $2\pi\rho_w^{-1}(2RT_w)^{3/2}f$ at $Kn_w = 0.1$ (II); the transition region to free molecular region. (a) $r/L = 5.141$, (b) $r/L = 20.96$, and (c) $r/L = 102.9$.

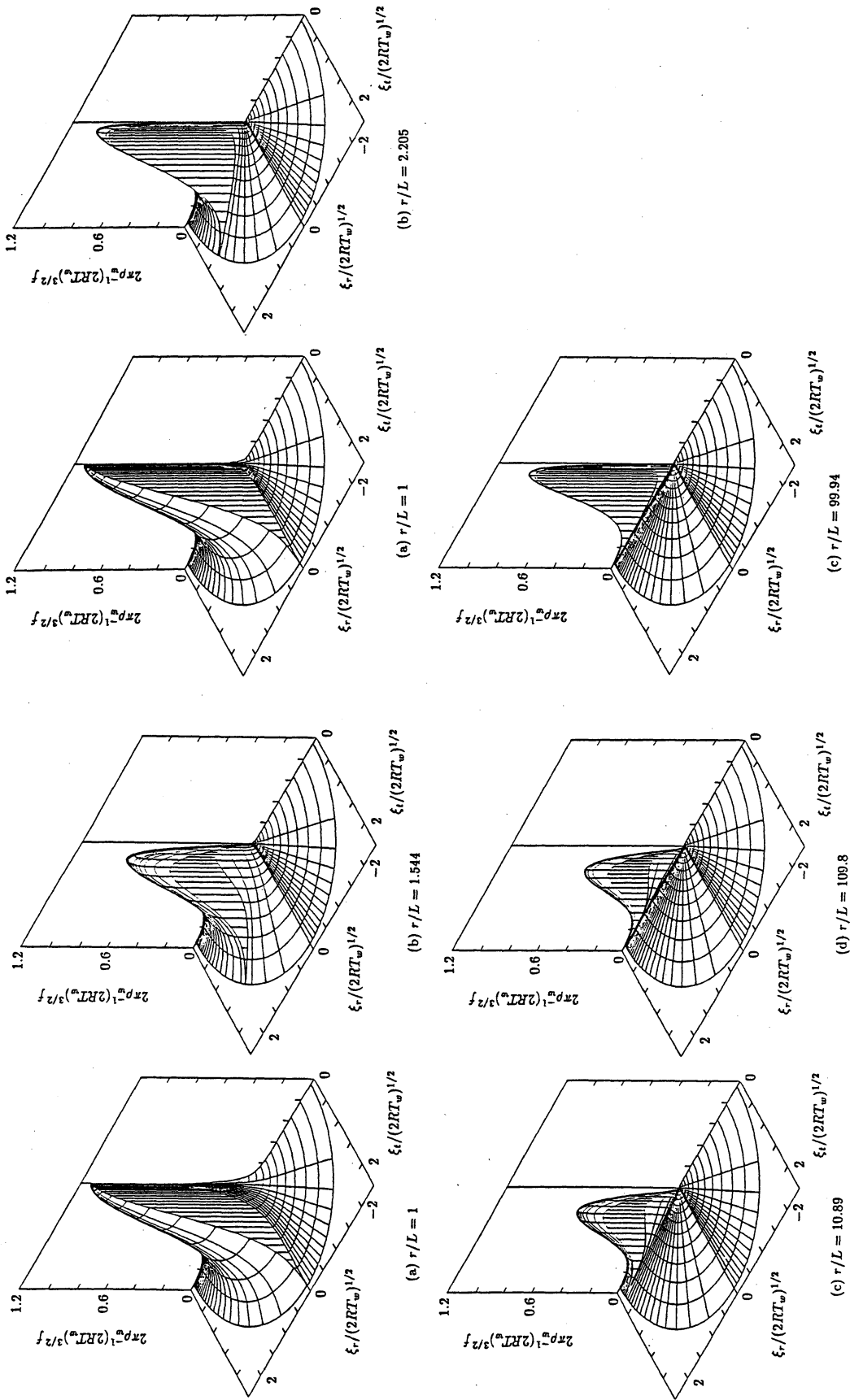


FIG. 10. The nondimensional velocity distribution function $2\pi\rho_w^{-1}(2RT_w)^{3/2}f$ at $Kn_w = 1$. (a) $r/L = 1$, (b) $r/L = 1.544$, (c) $r/L = 10.89$, and (d) $r/L = 109.8$.

FIG. 11. The nondimensional velocity distribution function $2\pi\rho_w^{-1}(2RT_w)^{3/2}f$ at $Kn_w = 10$. (a) $r/L = 1$, (b) $r/L = 2.205$, and (c) $r/L = 99.94$.

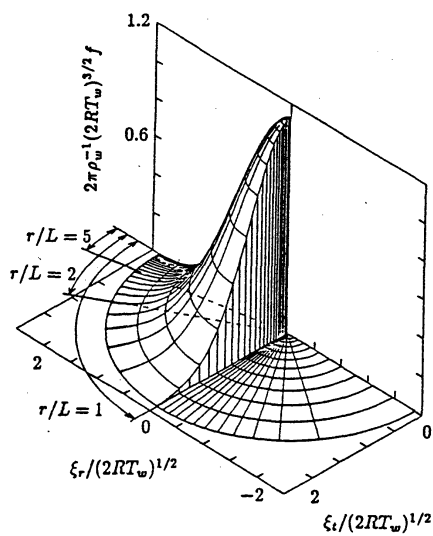


FIG. 12. The nondimensional velocity distribution function $2\pi\rho_w^{-1}(2RT_w)^{3/2}f$ at $Kn_w = \infty$. The distribution is the part $\xi_r/\xi > [1 - (L/\tau)^2]^{1/2}$ of the function $2\pi^{-1/2} \exp(-\xi^2/2RT_w)$.

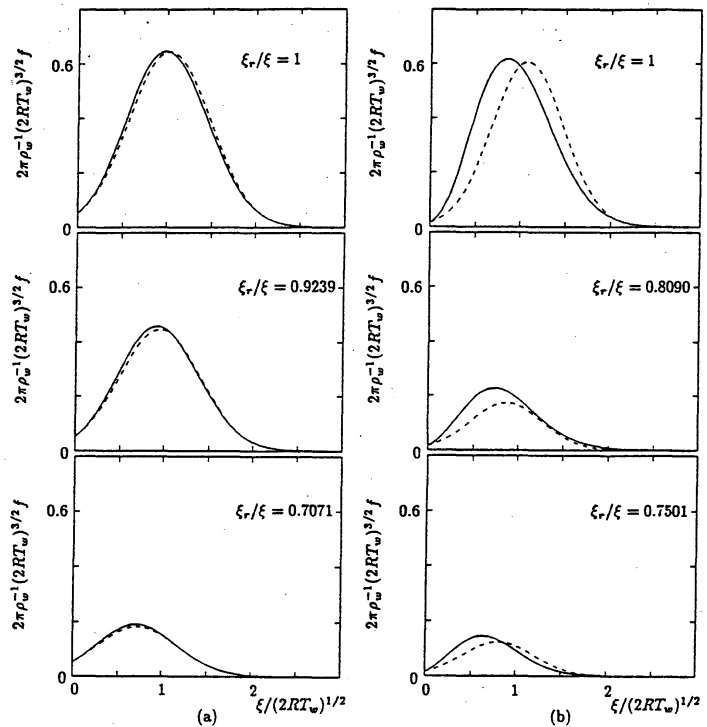


FIG. 13. Comparison with the local Maxwellian. (a) $Kn_w = 0.01$ and $r/L = 1.264$; (b) $Kn_w = 0.1$ and $r/L = 1.627$. The dashed line represents the local Maxwellian $2\pi\rho_w^{-1}(2RT_w)^{3/2}f_e$. The f_e has the same density, flow velocity, and temperature as f . The f in (a) corresponds to Fig. 7(a) and \bullet in Fig. 15, and that in (b) to Fig. 8(c) and \circ in Fig. 15.

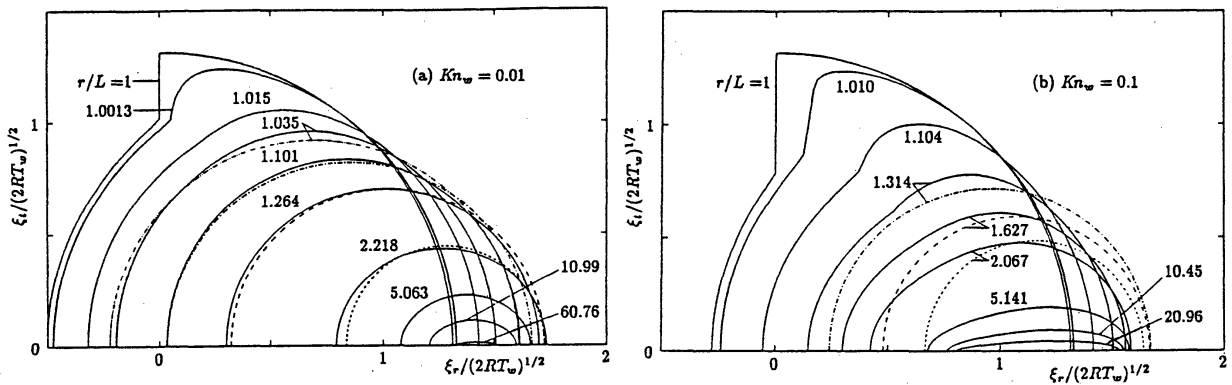


FIG. 14. The contour of $2\pi\rho_w^{-1}(2RT_w)^{3/2}f = 0.2$ for various points r/L . (a) $Kn_w = 0.01$ and (b) $Kn_w = 0.1$. The contour of the local Maxwellian is shown by: \cdots [$r/L = 1.035$ ($Kn_w = 0.01$)], \cdots [$r/L = 1.101$ ($Kn_w = 0.01$), 1.314 ($Kn_w = 0.1$)], \cdots [$r/L = 1.264$ ($Kn_w = 0.01$), 1.627 ($Kn_w = 0.1$)], and \cdots [$r/L = 2.218$ ($Kn_w = 0.01$), 2.067 ($Kn_w = 0.1$)]. The dashed line \cdots corresponds to Figs. 7(a) and 13(a) ($Kn_w = 0.01$) or Figs. 8(c) and 13(b) ($Kn_w = 0.1$). The flow deviates considerably from the local Maxwellian over the whole field when $Kn_w = 0.1$.

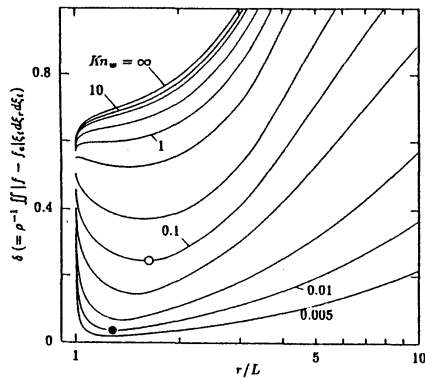


FIG. 15. $\delta (= \rho^{-1} \iint |f - f_e| \xi_i d\xi_r d\xi_t)$ versus r/L . The symbols \bullet and \circ correspond to Figs. 13(a) and 13(b) respectively. The δ is a measure of deviation of the flow (f) from the local Maxwellian distribution (f_e) ($\delta = 0$ when $f = f_e$, and $\delta = 2$ when f and f_e are disjoint).

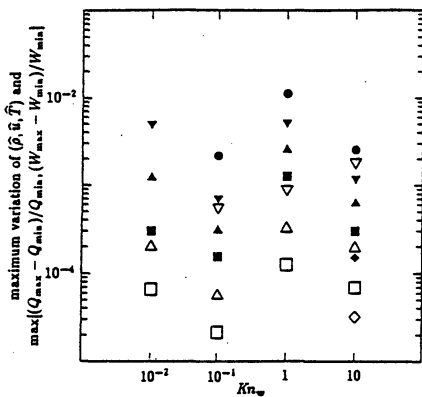


FIG. 17. The $\tilde{r}\theta_\zeta$ lattice dependence of $(\hat{\rho}, \hat{u}, \hat{T})$, $(Q_{\max} - Q_{\min})/Q_{\min}$ and $(W_{\max} - W_{\min})/W_{\min}$. The maximum variation of $(\hat{\rho}, \hat{u}, \hat{T})$ over the whole lattice points on $1 \leq \tilde{r} \leq \tilde{r}_D$ for different numbers I and (K, \bar{K}) of the $\tilde{r}\theta_\zeta$ lattice points are marked with hollow symbols. The $\tilde{r}\theta_\zeta$ lattice dependence of $\max[(Q_{\max} - Q_{\min})/Q_{\min}, (W_{\max} - W_{\min})/W_{\min}]$ is marked with black symbols. Let LS be the $\tilde{r}\theta_\zeta$ lattice system, described in the first paragraph in Sec. V D, with which the results in Sec. V A, B, and C are obtained (Note that it depends on Kn_w). M_0 is the same lattice system as LS for $Kn_w = 0.01, 0.1, \text{ and } 10$, and M_0 is that with double (K, \bar{K}) of LS for $Kn_w = 1$. M_n is a test lattice system with double I and (K, \bar{K}) of those of M_{n-1} . The ∇ indicates the maximum variation of $(\hat{\rho}, \hat{u}, \hat{T})$ between M_{-3} and M_{-2} lattices; Δ between M_{-2} and M_{-1} ; \square between M_{-1} and M_0 ; \diamond between M_0 and M_1 . The \bullet indicates $\max[(Q_{\max} - Q_{\min})/Q_{\min}, (W_{\max} - W_{\min})/W_{\min}]$ for M_{-3} ; \blacktriangledown for M_{-2} ; \blacktriangle for M_{-1} ; \blacksquare for M_0 ; \blacklozenge for M_1 . From separate tests, the results \square and \blacksquare are not influenced if LS is taken as M_0 for $Kn_w = 1$.

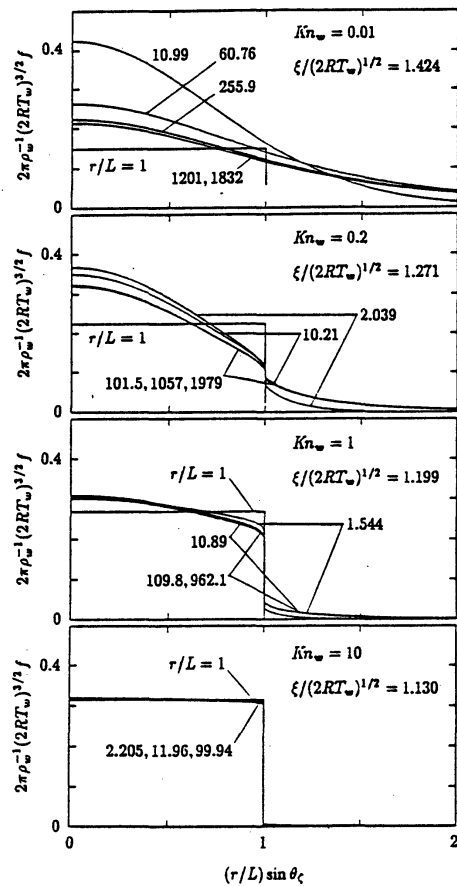


FIG. 16. The nondimensional velocity distribution function $2\pi\rho_w^{-1}(2RT_w)^{3/2}f$ at some $\xi/(2RT_w)^{1/2}$ versus $(r/L)\sin\theta_\zeta$ ($\theta_\zeta \leq \pi/2$) for various r/L .